Development and Validation of a Nanodosimetry-Based Cell Survival Model for Mixed High- and Low-LET Radiations

A Thesis
Presented to
The Academic Faculty

by

Xin Zhang

In Partial Fulfillment
of the Requirements for the Degree
Doctor Philosophy in the
Woodruff School of Mechanical Engineering

Georgia Institute of Technology
August 2006

Development and Validation of a Nanodosimetry-Based Cell Survival Model for Mixed High- and Low-LET Radiations

Approved by:

Dr. C.-K. Chris Wang, Advisor
NRE/MP Program
School of Mechanical Engineering
Georgia Institute of Technology

Dr. Nolan E. Hertel
NRE/MP Program
School of Mechanical Engineering
Georgia Institute of Technology

Dr. Farzad Rahnema
NRE/MP Program
School of Mechanical Engineering
Georgia Institute of Technology

Dr. Harish Radhakrishna
School of Biology
Georgia Institute of Technology

Dr. Mohamad Al-Sheikhly
Chemical and Nuclear Engineering Department
University of Maryland

Date Approved: 06/01/2006

ACKNOWLEDGEMENTS

I am deeply grateful to Dr. Chris Wang who is not only my advisor but also my mentor both in my academic and in my personal life. I thank him for giving me this wonderful opportunity to work with him throughout my PhD study. His guidance, support, patience and encouragement have made the completion of this project possible. I wish to thank Dr. Harish Radhakrishna for providing me his lab facility to learn cell culture and his former student, Dr. Murph Mandi, who taught me how to grow cells. I also want to express my appreciation to Drs. Nolan E. Hertel and Farzad Rahnema for taking the time to provide assistances to this research.

I wish to thank Dr. Mohamad Al-Sheikhly for his full support and for giving me the opportunity to use the University of Maryland (UOM) nuclear reactor facilities for conducting the cell experiment. I also want to thank Ian Gifford and Vincent G. Adams of UOM for helping me run the cell experiments. It has been an adventure for me, and I could not have made it without them.

I want to give my special thanks to Eric Burgett: Thank you for helping me calculate the fission neutron spectrum with MCNP5 and for providing the technical support that was needed in this project. I would also like to express my gratitude to Nazia Zakir: Thank you for your advice; you have helped me in many ways. I also would like to acknowledge my dear colleagues in the ORS office, Jermiah Sauber and Arlene Smith, it has been a great pleasure of working with you.

To my husband, Yuangang Xiang: I am so lucky to have you as my life partner who understands me so well and has fully supported me in everything, especially in this

PhD Study. To my son, Daniel Xiang, who has brought so much pleasure into my life: you are my motivation to be successful both academically and as a mother.

TABLE OF CONTENTS

LIST OF TABLES

Page No.

LIST OF FIGURES

Page No.

SUMMARY

A new nanodosimetry-based cell survival model for mixed high- and low-LET radiation has been developed. The new model employs three dosimetry quantities and three biological quantities. The three dosimetry quantities are related to energy depositions at two nanometer scales, 5nm and 25nm. The three biological quantities are related to lesion production and interaction probabilities, and lesion repair rate. The model assumes that the lesions created at the two nanometer scales are directly or indirectly responsible for cell death depending on the lesions' interaction and repair rate. The cell survival fraction derived from the new model can be expressed by the familiar dose-dependent linear quadratic formula, $\alpha D + \beta D^2$. The coefficients α and β are based on the three nanodosimetry quantities and the three biological quantities.

Validation of the new model has been performed both by using published data and by the experimental data obtained. Published cell survival curves for V-79 Chinese hamster cells irradiated with various LET of radiations were used for validation. Cell survival experiments were performed using V-79 cells irradiated with ^{60}Co gamma-rays with different dose rates to verify the validation results using the published data. The new model was applied to radiation therapy by irradiating V-79 cells with mixed fission neutron and gamma-rays. The validation results showed that this new model can be used to predict the cell survival and synergistic effect for mixed high- and low-LET irradiation.

CHAPTER 1

INTRODUCTION

Studies on cell survival under mixed low- and high-LET radiation have been of great interest to radiation biologists both scientifically and pragmatically [1-4]. On the scientific front, the prediction of cell response to a mixed radiation field poses a great challenge because it requires a detailed understanding of the mechanisms by which a cell is killed by radiation at the cellular and sub-cellular levels. Pragmatically, there is a need for the ability to predict of the tissue response for several new radiation therapy modalities that use mixed LET radiation [5].

Most experimental results have shown that the low-LET radiation and high-LET radiation do not act independently and that synergistic effects exist between the two types of radiation. Attempts have been made to use various cell survival models to predict the synergistic effects [6-8]. Through the last six decades, the cell survival models have evolved from a simple mathematical exercise of the target theory presented in 1949 to the latest microdosimetry-based models that include the complex lesion interactions and repair processes [9-14]. Many of these models were used to predict radiation effects other than cell survival fraction, namely the yield of DNA double strand breaks and various types of chromosome aberrations. Generally speaking, the development of biophysical models is hampered by poor understanding of the nature of the radiation-induced lesions, their repair kinetics and interactions at the DNA and chromatin levels.

In the last decade or so, numerous studies have been reported on the initial spectrum of radiation-induced DNA lesions, their repair mechanisms and kinetics, and

how they are related to cell death [15-26]. To keep abreast of the latest knowledge, this thesis presents a new nanodosimetry-based cell survival model that can be applied to predict the cell survival fractions for mixed high- and low-LET radiations.

This thesis has two major goals. The first goal is to develop a new cell survival model which can predict the survival fractions caused by a mixed high- and low-LET radiation field. The second goal is to validate the new model with experimental results obtained using V79 Chinese hamster cells. The thesis is presented in eight chapters. Chapter 2 gives a literature review on a few important subjects in cellular radiation biology including the various cell survival models. The new nanodosimetry-based cell survival model is then presented in Chapter 3. Chapter 4 presents the model validation method that employs the previously published cell survival data. Chapter 5 describes the experimental facilities and presents the computational and experimental methods and results for obtaining the relevant dose quantities for the V79 cell survival experiment. The actual cell survival experiment and results are presented in Chapter 6. Chapter 7 presents the application of the new model to radiation therapy. Conclusions and recommendations for future work are presented in Chapter 8.

CHAPTER 2

LITERATURE REVIEW

2.1 Radiation Induced DNA Lesions

The radiation damage to the DNA molecule is believed to be directly responsible for causing death to the irradiated cells. Two general classes of interactions of radiation with DNA can be identified: direct and indirect actions. The direct action refers to when the energy of a radiation particle is directly absorbed by the DNA molecule and cause damage. The indirect action refers to when the energy of a radiation particle is absorbed by the solvent molecules (e.g. water) to produce reactive species (e.g. free radicals), which in turn diffuse and react with DNA. Ionizing radiations are known to produce many different types of molecular damage to DNA, such as DNA single strand breaks (SSB), DNA double strand breaks (DSB), DNA protein cross links and base damage pathway, etc.[27] Over the past two decades emphasis has shifted to DSBs as the critical damage for radiobiological effects. It has been indicated that the biological consequences of ionizing radiation are determined by their clustering properties at the level of the DNA duplex [28]. The current picture of radiation induced DSBs, the distribution of DSBs, and the relationship between the radiation quality and the DSBs are reviewed in this section.

2.1.1 DSBs induced by Low-LET Electrons and Photons

For low-LET electrons, the majority of hits in DNA do not lead to damage in the form of strand breaks. When strand breaks do occur, there are far more SSBs than DSBs. Among the DSBs, most are simple double strand breaks (sDSBs) – i.e. two SSBs occur on opposite strands within 10 base pairs (bps); a small (but significant) portion of these are complex double strand breaks (cDSBs) – i.e. a sDSB accompanied by at least one additional strand break within 10 bps [29].

It was shown by V. Michalik [30] that electrons with energies between 200 and 500 eV are most effective in producing DSBs, especially cDSBs. Because these electrons deposit all their energy within a distance of 5-10 nanometers, this clearly reflects the fact that the ion clusters (of high ionization density) of the size of a few nanometers are highly effective in producing DSBs and cDSBs. Figure 2.1 shows the yields of DSBs and cDSBs as a function of electron energy.

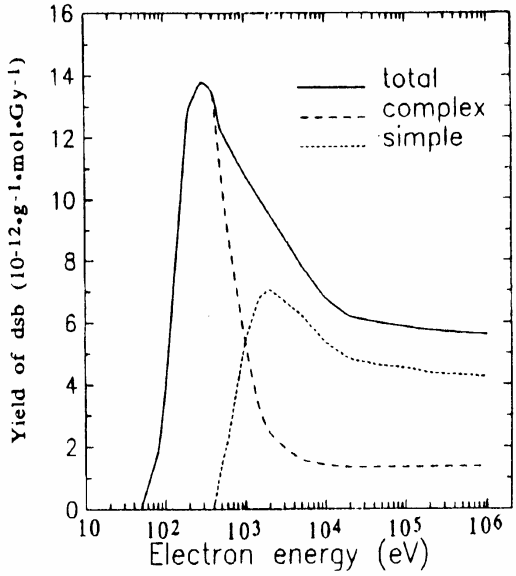

Figure 2.1. Yield of double-strand breaks produced in electron tracks as a function of the initial electron energy E_0. Total DSB (solid line), simple DSB(short dashed line), Complex DSBs(long dashed line). Adopted by V. Michalik

The above finding is further strengthened by studies on DNA lesions performed with the ultrasoft X-ray [15, 31-32]. These studies showed a large RBE value for the carbon K-shell ultrasoft X-ray when compared to a typical low-LET irradiation (e.g. with ^{60}Co gamma ray). In fact, the cell survival curve of the carbon K-shell X-ray is very similar to that of high-LET radiations. Studies also found that the yield of DSBs produced by the oxygen K-shell X-ray is roughly the same as that produced by typical low-LET gamma rays.

The above findings, therefore, indicate that it is the cDSBs (not the sDSBs) that are mostly responsible for cell death. It has been estimated that the mass density of inner-shell photoionizations is 1.6 times larger than that in the plasmid DNA for the same average dose to the sample [33-34].

2.1.2 DSBs Induced by High-LET Particles

Experimental results have shown that while the efficiency for cell killing significantly increases with increasing LET, the yields of DSB per unit dose remain similar or may even decrease [35]; but the yield of complex DSB per unit dose is proportional to the LET. H.Nikjoo et al.[36] showed that nearly 30% of DSBs are of complex form for low-LET radiation, but this rises to about 70% for high-LET radiation. The dominant feature associated with high-LET radiation was found to correspond to a class of ion clusters in nucleosome size targets (i.e. 5-10 nanometers in diameter) [37]. This finding is consistent with that obtained from the low-LET studies – i.e. the cDSBs (not the sDSBs) are mostly responsible for cell death. In addition, the cDSBs are mostly produced by the ion clusters of the size of 5-10 nanometers.

Other studies showed that, although the number of DSBs does not change with increasing LET, the number of DNA fragments produced during high-LET irradiation is proportional to LET and the spatial distribution of DSB and fragments induced by high-

LET radiations is non-random [38]. Due to the spatial correlation of ionization clusters along a high-LET particle track, and with the periodicity of DNA folding on all levels of chromatin organization in the cell, short and medium sized DNA fragments are almost certainly produced; and there is an increased probability that short and medium-sized DNA fragments will form with increased high-LET irradiation. So compared with low-LET radiation, high-LET radiations generate more clustering on all scale levels (from the nanometer to the micrometer). Consequently, the damage by high-LET radiations is much more complex. In addition, because many DNA lesions along a high-LET particle track are spatially very near one another, many of the adjacent DNA lesions interact with each other to form more complex lesions on the chromatin fiber level, which has a diameter of 25- 30 nm. [39-41]

2.2 Repair Mechanisms for DSBs

There are two known cellular mechanisms for repairing DSBs: homologous recombination and nonhomologous recombination. Homologous recombination requires an undamaged DNA strand as a participant in the repair. The nonhomologous repair is simply an end-to-end rejoining recombination, which, therefore, is an error-prone process and probably accounts for many of the premutagenic lesions induced in the DNA of human cells by ionizing radiation. Regardless of its error-prone nature, nonhomologous end joining (NHEJ) is the major repair pathway for DSBs in mammalian cells [42]. The time-course of NHEJ repair has generally been described as being biphasic and the half-times of the two phases differ for different cell lines. Typically the average half-time of these two phases were 5-30 minutes and 1-3 hours, respectively, and are independent of LET [43-44]. The majority of DSBs were rejoined by the fast phase, but the fraction of DSBs rejoined by the slow phase and the fraction of unrejoined DSBs at 20-24 hours increased with increasing LET. [45]

Lobrich, Rydberg, Cooper and their colleagues, [46-48] have used the restriction fragment sizes combined with the pulsed-field gel electrophoresis and obtained a good measure of rejoining relative to misrejoining. They found that the repair kinetics was generally slower after irradiation with high-LET particles when compared to X-ray irradiation and that a larger proportion of the DSBs remained unrepaired after 24 hours.

Also, with increasing LET the correct amount of end rejoining decreased. This indicates that as the complexity of the DSB increases, repair by NHEJ becomes severely inhibited [49].

2.3 Mechanisms of Radiation-Induced Cell Death

There are three different mechanisms of cell death: necrosis, apoptosis, and mitosis linked cell death. While the first two mechanisms directly result in the actual cell decomposition, the third mechanism does not.

Necrosis is an acute pathological cell death. It generally results from cell injury or from lack of oxygen or essential metabolites, and it is characterized by a tendency for cells to swell and ultimately lyses. This, in turn, allows the cell's contents to flow into the extracellular space. At the tissue level, necrosis is usually accompanied by an inflammatory response.

Apoptosis is also called programmed cell death; it is characterized by a stereotyped sequence of morphologic events. It involves shrinkage of the nucleus and cytoplasm, followed by fragmentation and phagocytosis of these fragments by neighboring cell or macrophages. As a mode of radiation-induced cell death, apoptosis is highly cell-type dependent.

Mitotic-linked cell death is often referred as the reproductive cell death. In this case, the body of the cell may still be present and apparently intact after irradiation, it may be able to make proteins or synthesize DNA or may even be able to struggle through

one or two mitoses; but as long as it has lost the capacity to divide indefinitely (as a lively cancer cell does), it is considered to be dead. Since the mitotic-linked death is most relevant to the in-vivo studies of cell survival in this study, it is hereafter used as a synonym for cell death.

Studies show that mitotic-linked cell death resulting from chromosomal aberrations is the main route of radiation-induced cell death and that the apoptosis occurring either before or shortly after the cells divide following irradiation is responsible for only a very small fraction of radiation-induced cell death [50].

2.4 Cell Survival Models

The earliest cell survival model was proposed and summarized by Lea in 1949 [9]. It has come to be widely known as the target theory of cell killing. The first version of the target theory is the single-target single-hit inactivation, which assumes that one hit in the single target will cause cell death, and it leads to the form of survival curve shown in Fig. 2.2A. The survival curve is exponential, and it is a straight line in a semi-logarithmic plot of survival fraction versus dose.

These straight line survival curves can only be found in the inactivation of viruses and bacteria. For most of the mammalian cell lines, they are only appropriate in describing the very sensitive human cells or in the very high LET radiations. So a more general version of the target theory, called multi-target single-hit inactivation, was developed. It proposes that just one hit by radiation on each of n sensitive targets in the cell is required for death of the cell. The survival curve is shown in Fig. 2.2B, and it is an ‘off the shoulder’ curve.

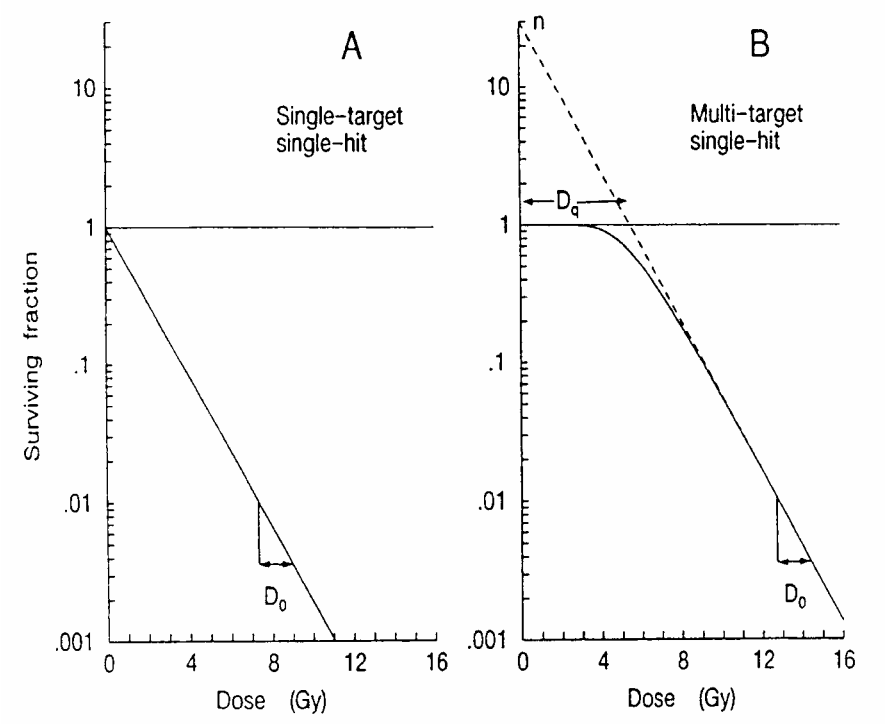

Figure2.2 The two most common types of target theory. A: single-target inactivation; B. Multi-target inactvation.

In the 1960's, as experience with mammalian cell lines grown in tissue culture increased, it became clear that many cell lines have survival data that do not agree with the formula described by the target theory [51-52].

In the 1970's and 80's, more models were proposed with the aim to account for DNA damage and to replace the target theory. A most noticeable characteristic of these models is that the cell survival fraction (S) of most of these models can be expressed as the linear-quadratic formula, i.e. $-\ln S = \alpha D + \beta D^2$, which is generally true for most of the mammalian cells for survival fractions greater than 10^{-3} [53]. Some of the representative models are described in the following paragraphs.

Most of the currently existing models can be referred as the binary lesion interaction (BLI) models. The idea of BLI was first brought up by Neary et al. in 1965 [54]. They assumed that two lesions may interact to form aberration in a given volume and two lesions within a potential interaction distance may be obtained by either single particle traversal through the sensitive structures or by the passage of two particles. Most of the BLI models were developed between the early 1970's and the mid 1980's. The representative ones include repair-misrepair model (RMR) [12] , lethal-potential-lethal (LPL) [14] model, and the theory of dual radiation action (TDRA) model [55-56].

The RMR model directly deals with the DNA repair processes [12, 57]. It describes the yield of relevant macromolecular lesions per cell as a function of dose (D) (see Fig. 2.3). There is a time (t)-dependent transformation of these lesions, and accompanying time- and dose-dependent probabilities of survival(S), lethality (L), and mutation (M). The model also postulates a class of lesion U, which stands for the"uncommitted" lesion. There are many repair states that are the result of transformation of U lesions.

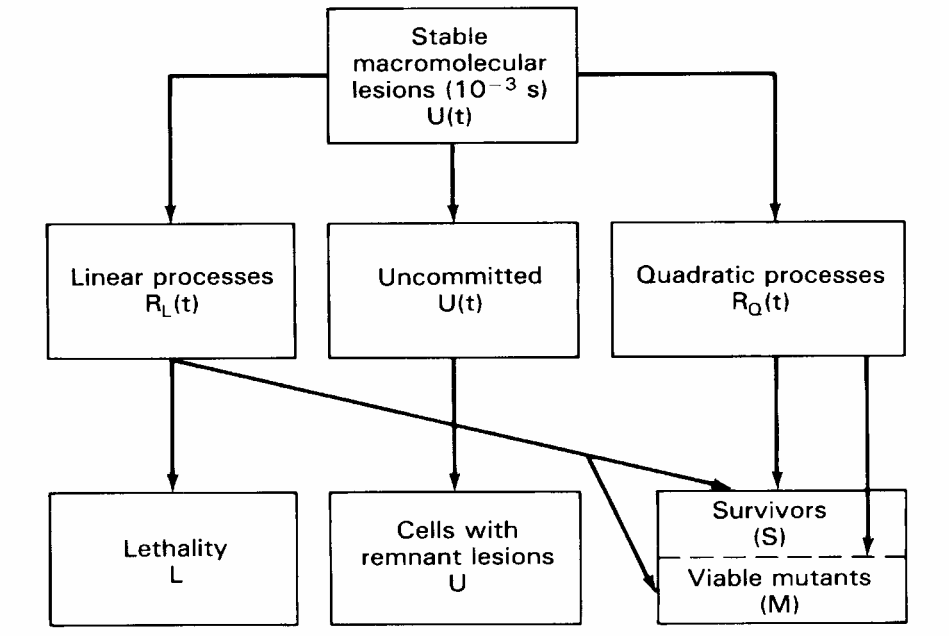

Figure 2.3 Repair-misrepair model

The LPL [14, 58] model proposes a unified repair of cell killing. As shown in Fig. 2.4, the model has two sensitivity parameters, η_L, which determines the number of non-repairable lesions produced per unit dose, and η_{PL}, which determines the number of repairable lesions. There are also two rate constants ε_{PL} and ε_{2PL}, the rate at which they undergo interaction and thus misrepair.

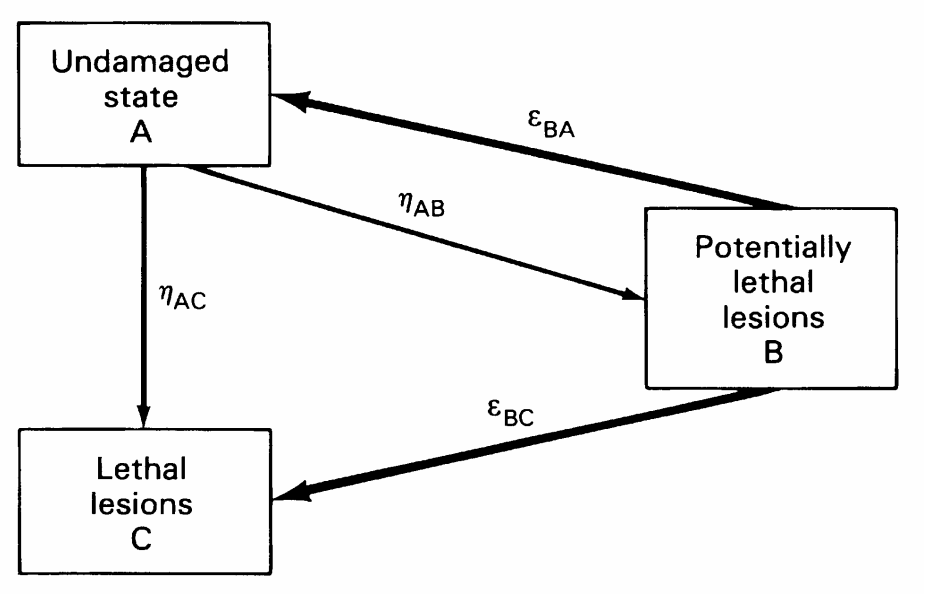

Figure 2.4 Lethal-potentially-lethal model

The LPL and RMR models present a class of kinetic (reaction rate) models that attempt to link radiation damage to higher level end points through biologically plausible first- and second-order repair processes.

The TDRA was first developed more than three decades ago as an attempt to explain the empirical observation of the large values of relative biological effectiveness (RBE) associated with high LET particles. Since then, the theory has been revised twice, with the latest version known as the theory of compound dual radiation action (CDRA) [59].

In the theory of CDRA, the primary lesions are the SSBs and two of them can interact and combine to form a DSB, which by itself can induce simple chromosome breaks, or a pair of DSBs can interact (or combine) to form so-called two-break chromosome aberrations in "compound dual radiation action". In each case, pairs of entities combine to form lesions that can cause injury or death of cells. Fig. 2.5 is a graphic description of the CDRA theory.

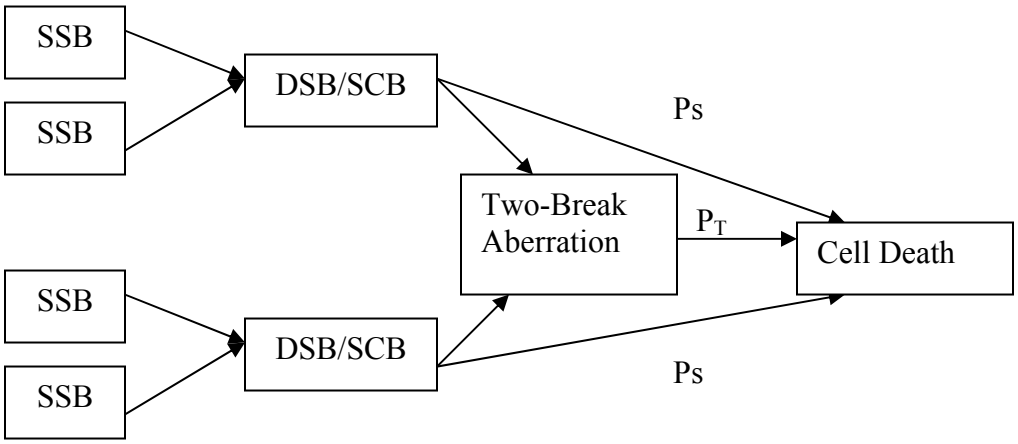

Figure 2.5 The CDRA cell survival model

The original TDRA included a microdosimetry quantity, and the CDRA theory made additional improvements by including microdosimetry quantities at two microscopic scales (5 nm and 1 μm) [60]. It has long been recognized that the ultimate biophysical model for cell survival must be based on microdosimetry quantities that include energy deposition, track structure, biomolecular targets, and cell repair mechanisms, etc [61]. The TDRA, however, has been under a great deal of criticism because it defines the dimensions of separation of the interacting sites in micrometer terms while biochemistry tells that the interactions cannot be separated by more than a few base pairs.

In addition to the BLI models, one other model called the repair saturation (RS) model also worth mentioning. The RS model proposed that the shape of the survival curve depends only on a dose-dependent rate of repair [13,62]. Only one type of lesion

and single-hit killing were postulated. As such, in the absence of any repair, these lesions produce the steep "single-target single-hit" survival curve. The final survival curve results from repair of some of these lesions. Under low-dose and low-dose-rate irradiations, there are plenty of repair enzymes available; and therefore, most of the damage can be repaired. Under high-dose and high-dose-rate irradiation, however, the repair enzymes become saturated so that many damages become fixed before they can be repaired. In other words, the "repair saturation", rather than the "lesion interactions assumed in the BLI models, is the cause of steeper slopes of survival curves for high-dose and high-dose-rate irradiations.

With the advent of the new cell and molecular biology techniques, e.g. the premature chromosome condensation (PCC) technique and the pulsed-field gel electrophoresis technique (FAR), much data has been obtained, especially the data related to the yield of strand breaks and the size distribution of DSB fragments [63]. More detailed cell survival models have recently been developed based on these new data. One of the representatives is called a track structure model. [31,37,64-65] Track structure, as a branch of theoretical physics, uses a quantity called 'cross-section' to represent the probability of these processes for the simulation of what actually happens in the medium. They use Monte Carlo track structure simulation code to follow the history of electron interactions in liquid water. The code follows the primary and all the secondary electrons generated in liquid water until they are thermalized, recording the coordinates of all inelastic interactions, the amount of energy deposited at the point of interaction, the type of interaction and the time of generation of initial radical species. Track structure models have successfully predicted the distribution of DNA lesions in cells such as the yield and distribution of SSBs, DSBs and clusters of DSBs. But to link these lesions to the cell death, more work still needs to be done.

Another recently developed cell survival model is called Two-Lesion Kinetic Model (TLK) [66-67]. This model extends and refines the formalism of the earlier LPL and RMR kinetic models. Detailed DSB rejoining processes are treated to better link biochemical processing of the double strand breaks to cell killing. A unique aspect of the TLK model is that break ends associated with both sDSB and cDSB are allowed to interact in pairwise fashion to form irreversible lethal and nonlethal damages. While TLK can be used to estimate the yield and distribution of DNA lesions, it does not predict the cell survival fraction especially for mixed high- and low-LET irradiation.

In summary, through the last six decades, the cell survival models have evolved from a simple mathematical exercise of the target theory presented in 1949 to the latest microdosimetry-based models that include the complex lesion interactions and repair processes [5,61,68-70]. Generally speaking, the development of cell survival models is still hampered by the lack of understanding of the nature of the radiation-induced lesions, their repair kinetics and interactions at the DNA and chromatin levels.

CHAPTER 3

THE NEW NANODOSIMETRY-BASED CELL SURVIVAL MODEL

3.1 Arguments on Cell Death Mechanisms

From Chapter 2, it is known that radiation induces DNA lesions and that the initial spectrum of the DNA lesions and their repair efficiencies are closely related to the radiation quality (i.e. RBE) and to the environment within the cell nucleus at the time of irradiation. But there is still a debate as to what is the precursor (or cause) that leads to chromosome aberrations and cell death. Most researchers believe that the DNA DSB is the key target that directly leads to chromosome aberrations and cell death. Others, however, believe that radiation damage not involving DNA could also be of crucial importance [71].

Hofer et al. [23-26] show clearly in their experiments that DNA damage alone is not sufficient to kill cells. In their studies, Chinese hamster ovary cells were synchronized at the G1/S-phase and were pulse-labeled with ^{125}I-iododeoxyuridine (a DNA precursor) 30 min after they entered the S phase. The ^{125}I is an auger emitter by electron capture emission and/or internal conversion. More than 99% of these emissions are low-energy electrons with a very short range in biological material. So the electron dose emitted from ^{125}I is deposited in a sphere with radius of about 40 nm around the decay site. It has been calculated that the radiation dose in the immediate vicinity of ^{125}I can exceed that deposited by a densely ionizing 5-MeV α particle with an LET of 100 keV/μm. The cell survival curves observed in Hofer's experiments, however, were the

same as the ones exposed to low-LET radiation within 1 hour after pulse labeling. This contradicts to the results of cell survival curves for high-LETs. So this suggests that damage to a non-DNA structure (e.g. nuclear matrix attachment site, proteins forming the base of the DNA loop domain, or a high-order chromatin structure at the chromosome backbone) is also involved in cell death.

While the biological nature of the radiation-induced subcellular lesions responsible for cell death is unclear, it is still possible to develop a cell survival model. The author argues that one only needs to take into consideration the two specific sizes of subcellular target, 5 nm and 25 nm, which have been identified to be most relevant to cell death. As such, several dosimetry quantities based on these two nanometer target sizes were incorporated into the formulation of the new cell survival model. The supporting arguments are presented below.

The notion that the target size of 5 nm in diameter is important in radiation-induced cell killing is supported by both physical and biological evidence. Physically, it is a well known that a majority of the irreparable damage caused by the low-dose-rate low-LET radiations is caused by the delta rays (i.e. secondary electrons) with energies between 200 eV and 500 eV. This is because these electrons deposit all their energies in short distances between 5 nm and 10 nm, and thus form ion clusters which, in turn, produce irreparable damage. Biologically, the fact that the ultrasoft X-ray is significantly more efficient in cell killing than the ^{60}Co gamma ray further asserts that ion clusters of 5 nm in diameter produced by 200-300 eV electrons are most relevant to cell death [72].

The notion that the target size of 25 nm in diameter is important in cell killing is also well supported. Several studies showed that clusters of DNA lesions distributed over a chromatin fiber, which is around 25 nm in diameter, give rise to kilobase-sized DNA fragments (small and medium size fragments), and the yield of these DNA fragments per unit dose is proportional to LET of the radiation. This finding is consistent with the fact that 5-nm-diameter ion clusters are closely spaced along a high-LET particle track

resulting in closely spaced lesions, which in turn, may interact to form a 25-nm-diameter (or kilobase-sized DNA fragments) lesion. One more evidence is from the comparison of the cell survival curves of α particles with those of ultrasoft X-ray. While the mean energy deposition in a 5-nm-diameter target of α particles is comparable to that of ultrasoft X-ray, the slopes of α-particle survival curves are significantly steeper than that of ultrasoft X-ray, suggesting that two nearby 5-nm-diameter lesions may interact or combine to form a high-order lesion (i.e. 25 nm in diameter).

3.2 Premises

The new model is based on the following six premises:

Premise (1). There are three independent routes leading to cell death. As shown in Fig. 3.1, all three routes start with the 5-nm lesions produced by the ion clusters and go through an intermediate stage of chromosome (or chromatid) break (CB). Specifically, route 1 corresponds to a CB directly resulting from a 5 nm lesion; route 2 corresponds to a CB resulting from the combination of (or interaction between) two nearby lesions produced by the same radiation track (represented by the dashed box in Fig. 3.1); and route 3 corresponds to a CB resulting from the combination of (or interaction between) two distant lesions produced by two separate radiation tracks.

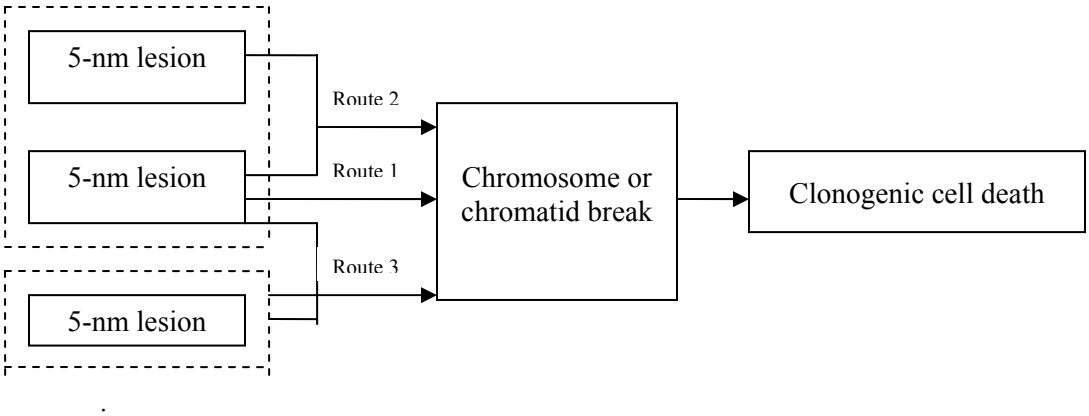

Figure 3.1 Various routes leading to cell death

Premise (2). There are two types of 5 nm-diameter lesions: the irreparable lesion (IL) and the reparable lesion (RL). The number of ILs in a cell via route 1 is linearly proportional to both the absorbed dose, D, and the nanodosimetry-based probability, F_1, defined by

$$F_1 = \int_{200\ \text{eV}}^{\infty} f(\varepsilon)\, d\varepsilon \qquad (3.1)$$

where $f(\varepsilon)$ is the single-event frequency distribution function of energy deposition, ε, per unit dose in a 5 nm x 5 nm cylindrical target.

Premise (3). The repair mechanism of the RLs follows one-compartment kinetics.

Premise (4). The number of CBs produced is linearly proportional to the number of ILs.

Premise (5). The number of ILs produced via route 2 is linearly proportional to both the absorbed dose, *D*, and the nanodosimetry-based probability, F_2, defined by

$$F_2 = \int_{1\,\mathrm{k\,eV}}^{\infty} f(\varepsilon)\, d\varepsilon \qquad (3.2)$$

where $f(\varepsilon)$ is the single-event frequency distribution function of energy deposition, ε, per unit dose in a 25 nm x 25 nm cylindrical target.

Premise (6). The number of ILs produced via route 3 is proportional to the square of the total number of randomly distributed RLs integrated over time. The number of RLs per cell is linearly proportional to both the absorbed dose, *D*, and the nanodosimetry-based probability, F_3, defined by

$$F_3 = \int_{100\ \mathrm{eV}}^{1\,\mathrm{keV}} f(\varepsilon)\, d\varepsilon \qquad (3.3)$$

where $f(\varepsilon)$ is the single-event frequency distribution function of energy deposition, ε, per unit dose in a 25 nm x 25 nm target.

Some of the above premises are self-explanatory. A few, however, need further justifications. The assertion in *Premise (1)* that a 5 nm-diameter lesion can lead to a CB is supported by the experimental cell survival curves of the ultrasoft carbon K-shell X-rays of which the photoelectrons have ranges less than 7 nm, as discussed in the last section[40,74-75]. Another assertion in *Premise (1)*, that two distant lesions are able to form a CB, is consistent with the recent study on interchromosomal interactions [76]. It is note worthy that, while routes 2 and 3 both involve interactions of two lesions, the two routes are treated separately. This is because in route 2, the interaction rate of two nearby lesions of the same radiation track are more-or-less instantaneous and therefore, independent of dose rate. In route 3, however, the interaction rate of two distant lesions of two separate radiation tracks may take minutes to hours, depending on both the

distances between two lesions and the cell repair rate, and is, therefore, dependent on both the absorbed dose and the dose rate. In *Premise (2)*, the threshold of 200 eV for F_1 is deliberately chosen to account for the fact that the randomly distributed 278-eV photoelectrons from carbon K-shell X-rays are lethal [40,75-76] and for the possibility to cause complex DSB. In *Premise (5)*, F_2 is introduced to assert that a high-LET radiation track, due to its closely-spaced ion clusters, tends to produce nearby lesions which are likely to combine (or interact) and form a CB [77]. In addition, the target size of 25 nm x 25 nm (~ the diameter of a chromatin fiber) is chosen to match the kilobase-sized DNA fragments characteristic to damages produced by high-LET heavy ions [20-22]. The threshold of 1 keV is chosen so that the target with a diameter of 25 nm will consist of several nearby lesions caused by the closely-spaced ion clusters [77]. In *Premise (6)*, the threshold of 100 eV for F_3 is characteristic of reparable DNA damage [78]. The upper bound for F_3 is set at 1 keV to discount the closely-spaced lesions of a high-LET radiation track.

3.3 Mathematical Formulation

According to Premise (2), the number of ILs in a cell can be expressed as

$$N_{IL} = k_1 F_1 D \tag{3.4}$$

where k_1 is the proportionality constant. By incorporating Eq. (3.4) into *Premise (4)*, the number of CBs via route 1 can be expressed as

$$(N_{CB})_1 = p_1 N_{IL} = p_1 k_1 F_1 D = r_1 F_1 D \tag{3.5}$$

where p_1 is the proportionality constant, and $r_1 = p_1 k_1$.

According to *Premise (5)*, the number of CBs per cell produced via route 2 can be directly expressed as

$$(N_{CB})_2 = r_2 F_2 \, D \tag{3.6}$$

where r_2 is the proportionality constant.

The algebraic expression for the number of CBs produced via route 3 is more complex because one needs to first obtain the expression for the number of RLs. According to *Premise (6)* the production rate of RLs in a cell can be expressed as

$$\frac{dN_{RL}}{dt} = k_3 \, F_3 \, \dot{D} - \lambda \, N_{RRL} \tag{3.7}$$

where N_{RL} is the number of RLs per cell, k_3 is the corresponding proportionality constant, and λ is the repair time constant for the RLs. If one denotes T as the total irradiation time, then the solution of $N_{RL}(t)$ for $t > T$ can be found as

$$N_{RL}(t) = \frac{k_3}{\lambda} F_3 \dot{D} (1 - e^{-\lambda T}) e^{-\lambda (t-T)} \tag{3.8}$$

In the high-dose-rate case where $T \ll t$ and $\lambda T \ll 1$, Eq. (3.8) is reduced to

$$N_{RL}(t) = k_3 F_3 D \, e^{-\lambda t} \tag{3.9}$$

According to *Premise (6)*, the number of CBs for route 3 is proportional to $N_{RL}(t)^2$ integrated over the time period of interest, t', which is typically a few hours. That is,

$$(N_{CB})_3 = \int_0^{t'} \nu\, N_{RL}(t)^2\, dt$$

$$= \frac{\nu\, k_3^{\,2}}{2\lambda}(1 - e^{-2\lambda t'})\, F_3^{\,2} D^2$$

$$= r_3 F_3^{\,2} D^2 \qquad (3.10)$$

where ν is a constant representing the interaction probability between two RLs of different radiation tracks, and

$$r_3 = \frac{\nu\, k_3^{\,2}}{2\lambda}(1 - e^{-2\lambda t'}) \qquad (3.11)$$

According to *Premise (1)* and Eqs. (3.5), (3.6), and (3.10), the total number of CBs can then be expressed as

$$N_{CB} = (N_{CB})_1 + (N_{CB})_2 + (N_{CB})_3$$

$$= \left(r_1 F_1 + r_2 F_2\right) D + r_3 F_3^{\,2} D^2 \qquad (3.12)$$

By comparing Eq. (3.12) with the classic linear-quadratic form, $\alpha D + \beta D^2$, one obtains

$$\alpha = r_1 F_1 + r_2 F_2 \tag{3.13}$$

and

$$\beta = r_3 F_3^{\,2} \tag{3.14}$$

In other words, α and β are expressed in terms of three biological quantities r_1, r_2, and r_3, and three physical quantities F_1, F_2, and F_3. It should also be noted that the inclusion of the time factors λ and t' in Eq. (3.10) indicates that r_3 is a function of cell repair rate. The above expressions of α and β are amenable to experimental validation using the vastly available cell survival data obtained from radiations of various LETs. Furthermore, the dose rate effect can also be examined with the above formula by replacing Eq. (3.9) with Eq. (3.8).

CHAPTER 4

VALIDATION OF THE NEW MODEL WITH PUBLISHED DATA

This chapter describes how previously published data was used to validate the new cell survival model proposed in Chapter 3.

4.1 Validation Method

As described in chapter 3, the new model can also be expressed as the linear quadratic model which is $\alpha D + \beta D^2$ and the α and β can be expressed in terms of three biological quantities r_1, r_2, and r_3, and three physical quantities F_1, F_2, and F_3. There is a unique character for these three biological parameters, which are cell type dependent and LET independent. So this character can be used to validate this new model. The three physical quantities also can be used to examine the shape of the cell survival curve.

Various V-79 cell survival curves, irradiated by different LET such as ultra-soft X-ray, X-ray, gamma ray, proton and alpha particles, were selected to validate the new model [72,79-82].

Since all the cell survival curves can be expressed as the linear quadratic formula, α and β values can be directly derived from the cell survival curves selected for the validation. The three physical parameters F_1, F_2, and F_3 can be directly obtained from the published data [83-85]

According to Equation (3.13), $\alpha = r_1 F_1 + r_2 F_2$, any two sets of values of α, F_1, and F_2 from two different survival curves selected can be used to uniquely determine r_1 and r_2. According to Equation (3.14), $\beta = r_3 F_3^{\,2}$, any one of the survival curves selected could give

a unique value of r_3. In reality, however, Equation (3.13) can only give reliable results for two survival curves with very different α values. This is because each survival curve contains an experimental uncertainty, and when two curves have similar α values, the resulting values of r_1 and r_2 become highly sensitive to experimental uncertainties. To avoid this problem, each of the two low-LET survival curves (the ^{60}Co gamma-ray or the 250-kVp x-ray) is coupled with one of the nine high-LET survival curves (the various energies of ultra-soft x-rays, protons, and alpha particles) to obtain a total of 18 sets of values of r_1 and r_2.

Similarly, Equation (3.14) can only give reliable values of r_3 from a survival curve with a significant "shoulder". This is because if βD^2 is much smaller than αD, the curve-fitted value of β would be unreliable, which, in turn, would make r_3 unreliable. To avoid this problem, only those survival curves that have reasonably large β values are used for determining r_3. The selected cell survival curves adopted from the published paper corresponding to different LET are in the Fig. 4.1. [72,79-82].

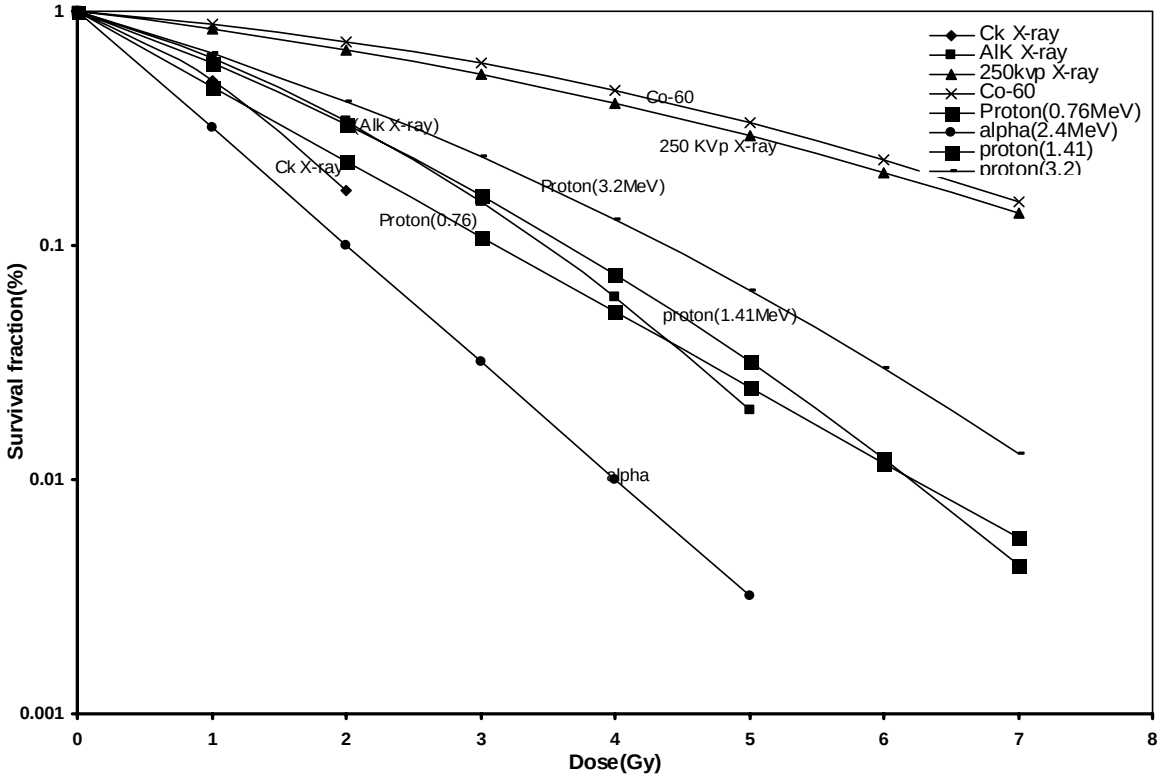

Figure 4.1. V-79 cell survival curves for radiations of various LETs

4.2 Validation Results

Table 4.1 shows the curve-fitted values of α and β for these published survival curves. Also included are the calculated values of F_1, F_2, and F_3 for the radiations of various LETs. Tables 4.2 and 4.3 show the values of three biological parameters r_1, r_2 and r_3 correspondingly.

Table 4.1. The values of α and β obtained from the published V79 survival curves and the calculated values of F_1, F_2, and F_3 for various radiation types. [72,79-82].

Radiation type	α (Gy^{-1})	β (Gy^{-2})	F_1 (Gy^{-1})	F_2 (Gy^{-1})	F_3 (Gy^{-1})
250 kVp X-ray	0.15	0.019	1.7×10^{-7}	6.8×10^{-7}	1.9×10^{-4}
^{60}Co γ-ray	0.10	0.024	1.2×10^{-7}	1.2×10^{-7}	1.6×10^{-4}
C_K X-ray	0.50	0.19	7.0×10^{-7}	0.0	3.2×10^{-4}
Al_K X-ray	0.38	0.081	4.5×10^{-7}	7.0×10^{-7}	2.1×10^{-4}
Ti_K X-ray	0.26	0.033	3.1×10^{-7}	8.0×10^{-7}	1.9×10^{-4}
0.64-MeV proton	0.65	–	6.43×10^{-7}	1.69×10^{-5}	1.28×10^{-4}
1.41-MeV proton	0.47	0.044	3.76×10^{-7}	6.45×10^{-6}	1.85×10^{-4}
3.2-MeV proton	0.37	0.036	2.71×10^{-7}	2.30×10^{-6}	2.33×10^{-4}
2.4-MeV α-particle	1.15	–	1.08×10^{-6}	2.68×10^{-5}	4.71×10^{-5}
3.8-MeV α-particle	1.32	–	1.13×10^{-6}	3.21×10^{-5}	6.72×10^{-5}
8.0-MeV α-particle	1.05	–	8.85×10^{-7}	3.14×10^{-5}	1.02×10^{-4}

Comparing α and β values from Table 4.1 for all different cell survival curves, the low-LET cell survival curves have lower α value than the high-LET radiation, but the Ck X-ray cell survival curve has a larger α value compared to the other low-LET irradiation. This can be explained by examining the corresponding F values.

First, Comparing the F_1 value of these different cell survival curves, the Ck X-ray has a larger F_1 value than the other lower LETs. The F_1 value is defined in the new model as in route 1 which is the energy deposited probability corresponding to the energy threshold from 200 eV and in 5 nm volume scale. The cluster ionization within 5 nm scale will cause the complex DSB and can cause the irrepairable lethal lesion; this is the reason why ultra-soft X-ray has a higher efficiency of cell killing compared to other low-LET cell survivals.

Second, comparing the F_2 value, the F_2 value is zero for ultrsoft X-ray, but for high-LET irradiation such as cell survival curves for alpha irradiation, F_2 is much bigger than the low-LET cell survival curves. The F_2 value is defined in the new model as in route 3 which is the energy deposited probability; corresponding to the energy threshold from 1keV and in the 25 nm volume scale. The heavy ion cluster within 25 nm will have the chance to interact each other and to cause the chromosome break which also can cause irreparable lethal lesion.

Third, comparing the F_3 value, F_3 is defined as the threshold probability from energy 100eV to 1keV. It includes the dose rate effect. Since only high dose rate was selected for this validation, the F_3 values are very similar to each other.

The calculated r_1, r_2 and r_3 values are listed in table 4.2 and 4.3.

Table 4.2: The values of r_1 and r_2 obtained from curve fit of various cell survival Curves [72,79-82].

Radiation type	r_1	r_2
^{60}Co γ-ray and C_K X-ray	7.14E+05	**1.19E+05**
^{60}Co γ-ray and Al_K X-ray	8.33E+05	**4.74E+02**
^{60}Co γ-ray and Ti_K X-ray	8.30E+05	**3.40E+03**
^{60}Co γ-ray and 0.64MeV proton	8.26E+05	7.02E+03
^{60}Co γ-ray and 1.41MeV proton	8.08E+05	**2.58E+04**
^{60}Co γ-ray and 3.2MeV proton	7.62E+05	**7.11E+04**
^{60}Co γ-ray and 2.4MeV α-particle	8.24E+05	9.72E+03
^{60}Co γ-ray and 3.8MeV α-particle	8.21E+05	1.22E+04
^{60}Co γ-ray and 8.0MeV α-particle	8.23E+05	1.02E+04
250 kVp X-ray and C_K X-ray	7.14E+05	**4.20E+04**
250 kVp X-ray and Al_K X-ray	8.90E+05	**1.85E+03**
250 kVp X-ray and Ti_K X-ray	7.59E+05	**3.07E+04**
250 kVp X-ray and 0.64MeV proton	8.59E+05	5.77E+03
250 kVp X-ray and 1.41MeV proton	7.71E+05	**2.79E+04**
250 kVp X-ray and 3.2MeV proton	4.52E+05	**1.08E+05**
250 kVp X-ray and 2.4MeV α-particle	8.47E+05	8.77E+03
250 kVp X-ray and 3.8MeV α-particle	8.36E+05	1.17E+04
250 kVp X-ray and 8.0MeV α-particle	8.44E+05	9.66E+03

Table 4.3. The values of r_3 obtained from curve fit of various cell survival curves[72,79-82].

Radiation type	r_3
250 kVp X-ray	1.06E+06
^{60}Co γ-ray	9.39E+05
Ti_K X-ray	9.22E+05
3.2-MeV proton	6.76E+05

Table 4.2 shows that the values of r_1 fluctuated very little, indicating that the choices of target size and threshold energy associated with F_1 are quite good. The values of r_2 and r_3, however, are not very consistent. These inconsistencies exist for the following reasons. First, since r_2 is related to the intra-track interaction (whose probability is represented by r_2), the r_2 values obtained from the soft X-rays and high energy protons are unreliable and should be discarded. Second, the cell survival curves used in this study are not perfect data for calculating these biological parameters. In fact, none of the curves that contain data for doses below 1 Gy. Consequently, the curve-fitted α values obtained from these curves cannot possibly be of high accuracy. If the α values are questionable, then the corresponding β values also become questionable. This explains the inconsistency among the r_3 values. Another factor causing the uncertainty of r_2 and r_3 has to do with the cell-cycle phases. This is because the cells used in these experiments were not synchronized in cell-cycle phases and because cells at different cycle phases have very different sensitivities to radiation.

By averaging all the r_1 values from Table 4.2, one obtains $r_1 = 8.15 \times 10^5 \pm$ 6.02%. By averaging all the reliable values of r_2 (i.e. with those in bold face discarded) from Table 4.2, one obtains $r_2 = 9.38 \times 10^3 \pm 23\%$. Although r_2 still has a large uncertainty, it does not greatly affect the accuracy of α, which is very much dominated by the accuracy of $r_1 F_1$. The average r_3 value is $7.67 \times 10^5 \pm 25\%$ for high-dose-rate irradiation, and the uncertainty of r_3 may be reduced in the future when more accurate cell survival data become available.

CHAPTER 5

EXPERIMENTAL FACILITIES AND DOSE EVALUATION

V-79 cell survival experiments were conducted to provide additional validation for the new cell survival model. V-79 cells were irradiated with two different radiation fields: a ^{60}Co gamma-ray field and a mixed neutron and gamma-ray field of a nuclear reactor. The ^{60}Co gamma-ray irradiation was conducted at the hot cell in the Neely Nuclear Research Center of Georgia Institute of Technology, and the mixed neutron and gamma-ray irradiation was conducted at the University of Maryland Training Reactor (MUTR).

In the ^{60}Co gamma-ray irradiation experiment, the cell flasks were placed at various distances from a NIST-traceable source whose corresponding dose rates were accurately measured and verified. Since the irradiation geometry is straightforward, no further description is necessary. This chapter mainly describes the irradiation facilities at the MUTR and discusses how the neutron and gamma ray dose components were determined.

5.1 Experimental Facilities

The MUTR is an open pool type reactor with a maximum licensed, steady state, thermal power of 250 kW. The reactor is fueled with 24 modified TRIGA fuel clusters. The reactor core consists of a total of 93 fuel rods - 20 fuel clusters each containing four fuel rods, one fuel cluster containing three fuel rods, an instrumented fuel rod, and the remaining three assemblies each contains three fuel rods and a control rod guide tube. The fuel rods are enriched to <20 w/o in ^{235}U, and each of the fuel rods contains a top and

bottom slug of graphite which act as reflectors. Additionally, two graphite reflector elements are positioned in the assembled core, adjacent to two of the outer fuel assemblies.

The reactor contains five experimental facilities. The graphite filled thermal column, the two (east and west) beam tubes, one through tube allowing relatively large samples to be placed adjacent to the core, and a pneumatic transfer system allowing small samples to be placed directly into the center of the core. The cross-sectional view of some of the MUTR components is shown in Fig. 5.1.

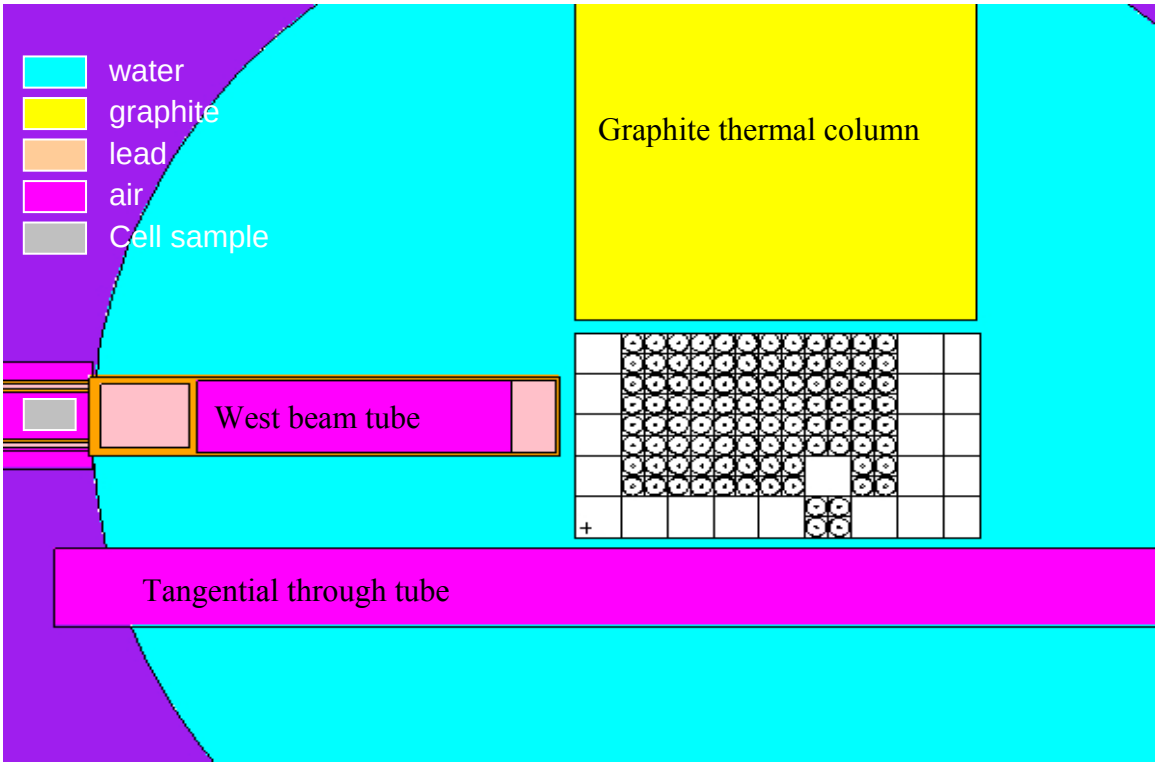

Fig. 5.1 Cross-sectional view of the MUTR Core

Before the actual cell irradiation experiment, several measurements were made to help decide the cell irradiation location. The selection of irradiation location was based on the following criteria: First, the total dose rate should be high enough so that the irradiation time is less than half an hour. This is because V79 cells usually cannot survive for more than an hour outside the incubator. Second, the total dose rate should be low enough so that the cell sample "transit time" is negligible in comparison with the irradiation time. Third, the neutron-to-gamma ray dose ratio should be high enough so that the high-LET effect can be clearly observed in the survival curves. It was judged that the west beam tube of the MUTR is the most appropriate location to carry out the mixed-field cell irradiation experiment. Since the neutron-to-gamma ray dose ratio was found to be low (much less than 1), a special beam insert was designed to attenuate gamma rays. The detailed dimensions and the front view picture of the beam insert are shown in Figures 5.2 and 5.3, respectively. Note that the beam insert with the cell sample is also shown in Fig. 5.1. As shown in Fig. 5.2, the lead shielding in the front end and around the outer layer of the beam insert effectively reduces the gamma-ray dose, and therefore, significantly increases neutron-to-gamma ray dose ratio.

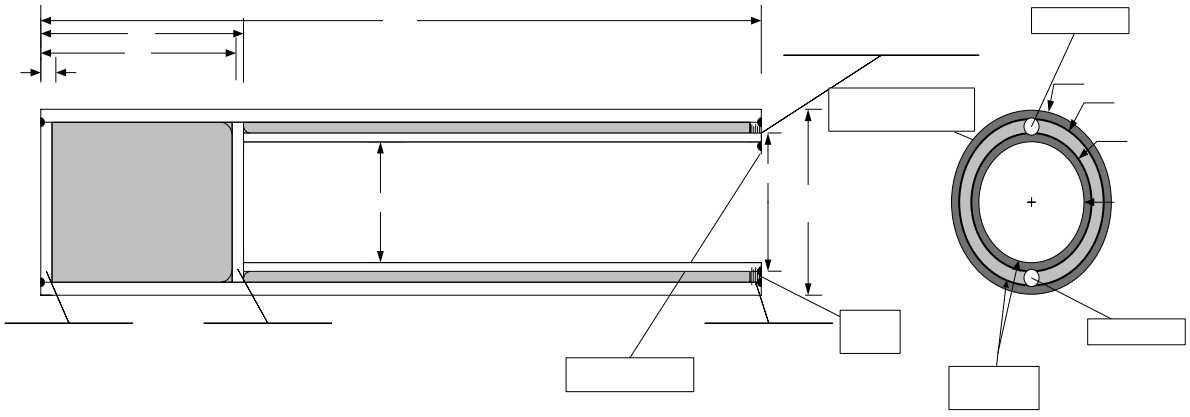

Figure 5.2 Detailed dimensions of the beam insert

6.75

6.50

0.50

Figure 5.3 Front view of the beam insert

5.2 Dual Ion Chamber Method

In order to accurately determine the neutron and gamma doses and dose rates, two miniature ion chambers made by Standard Imaging Inc. have been employed (see Fig. 5.4). The charge collecting volume is 0.056 cm^3 for both chambers. One of them, referred to by the vendor as M1, has its wall made of magnesium, which is almost only sensitive to gamma rays (i.e. its sensitivity to neutrons is extremely low). The other one, referred to by the vendor as T1, has its wall made of a tissue equivalent plastic (A150), which is sensitive to both neutrons and gamma rays. By using these two ion chambers together one will be able to "sort out" the neutron and gamma-ray doses in a mixed field.

Figure 5.4: Two miniature ion chambers T1 and M1

The general equation for the response (i.e. electric charge) of an ion chamber to a mixed field of neutrons and gamma-rays can be written in the following form [86]

$$Q_{n,\gamma} = AD_{\gamma} + BD_n \tag{5.1}$$

or

$$\frac{Q_{n,\gamma}}{A} = D_{\gamma} + \frac{B}{A} D_n \tag{5.2}$$

Where $Q_{n,\gamma}$ = total response due to the combined effects of the γ-rays and neutrons,

A = response per unit absorbed dose in tissue for γ-rays

B = response per unit absorbed dose in tissue for neutrons

D_{γ} = γ-ray absorbed dose in tissue

D_n = neutron absorbed dose in tissue

The gamma-ray calibration factor A can be obtained from a ^{60}Co gamma-ray beam whose the free-space exposure rate is known. The absorbed dose at the center of an equilibrium sphere of tissue, 0.52 g/cm^2 in radius, for a time run that produces a free-space exposure X (C/kg) at the same location, is given by the following equation [86]

$$D_{\gamma} = \beta \, A_{eq} \, X \, (\frac{\overline{W}}{e})_{air} \, (\frac{\mu_{en}}{\rho})_a^{tiss} \tag{5.3}$$

Where $\beta \cong 1.003$

A_{eq} = (attenuation of photons in penetrating to the center of the tissue sphere) $\cong 0.988$

$$(\frac{\overline{W}}{e})_a = 33.97 \text{ J/C}$$

$(\mu_{en}/\rho)_a^{tiss}$ = the ratio of mass energy absorption coefficients for tissue/air,

0.0293/0.0266=1.102

So equation (5.3) is reduced to

$$D_\gamma = 37.1\, X\ (Gy) \tag{5.4}$$

For the tissue-equivalent (TE) ion chamber, if $(Q_\gamma)_{TE}$ is the charge (C) produced in the ion chamber when it is given the same gamma-ray irradiation that deposits D_γ (Gy) in the tissue sphere, then

$$A_{TE} \equiv \frac{(Q)_{TE}}{D_\gamma} \text{ (C/Gy)} \tag{5.5}$$

Similarly, for the magnesium ion chamber, factor A_{mag} can be expressed as

$$A_{mag} = \frac{(Q_\gamma)_{mag}}{D_\gamma} \text{ (C/Gy)} \tag{5.6}$$

To obtain the neutron response B for both chambers, one uses the ratio of $\left(\frac{B}{A}\right)$ previously derived by Kuchnir et al.[87]. The ratio of $\left(\frac{B}{A}\right)$ as a function of neutron energy is shown in Fig. 5.5.

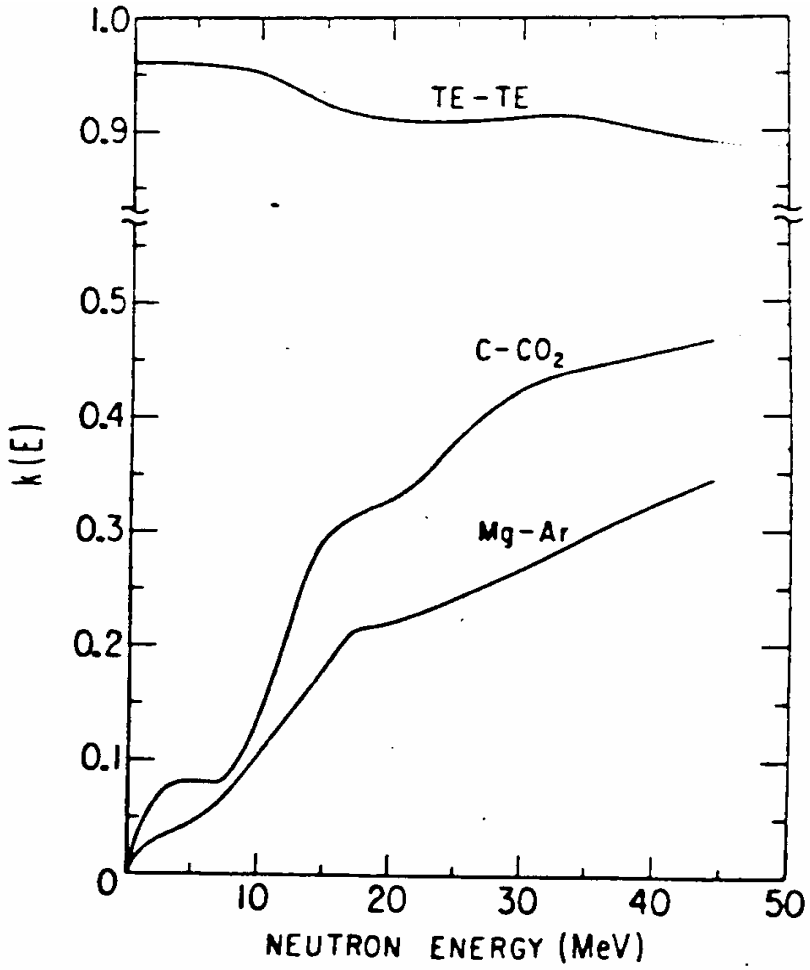

Figure 5.5 The ratio of $\left(\frac{B}{A}\right)$ as a function of neutron energy

5.3 Calibration of Ion Chambers Using Co-60 Source

The two ion chambers were calibrated with a NIST-traceable ^{60}Co source in the hot cell of the Neely Research Center at Georgia Tech. A digital electrometer (Model MAX-4000), made by Standard Imaging Inc., was used to measure the integrated charge over time. The calibration was conducted under two different gamma dose rates, 1.622 cGy/sec and 0.1014 cGy/sec. The calibration results are listed in Tables 5.1 and 5.2.

Table 5.1 The ion chamber calibration results for dose rate of 1.622 cGy/sec.

Ion Chamber Type	T1	M1
Dose rate (D_γ) cGy/sec	1.62	1.62
Charge produced(Q_γ) nC/sec	0.026±0.64%	0.03±0.49%
A_γ (nC/cGy)	0.016	0.018

Table 5.2 The ion chamber calibration results for dose rate of 0.1014 cGy/sec

Ion Chamber	T1	M1
Dose rate (D_γ) cGy/sec	0.10	0.10
Charge produced(Q_γ) nC/sec	0.0015±0.48%	0.0018±0.27%
A_γ (nC/cGy)	0.015	0.017

The above results show that gamma dose responses of these two ion chamber were different. The gamma response of T1 is slightly lower than the response of M1. Comparing the gamma dose response obtained by using high dose rate exposure and low dose rate exposure, there is a good agreement for the results of these two measurements. The difference between these two measurements is 6% for T1 and 4% for M1. The difference may be attributed to the charge leakage, which increases for the low dose rate exposure. The gamma responses for these two ion chambers are determined by averaging these two measurement results, and they are 0.01567± 4.4% nC/cGy for T1 and 0.0182 ± 2.68% nC/cGy for M1.

5.4 Dose Measurement of a Mixed Neutron and Gamma-Ray Field

The dual ion chamber method was used to determine the neutron and gamma-ray dose components inside the beam insert in the west beam tube of the reactor. The proper dose rate was obtained by adjusting the distance between the beam insert and the reactor core. The ion chamber responses at the final position inside the beam insert had the following readings: $Q_{n\gamma}^{TE}$ =0.019nC/sec and $Q_{n\gamma}^{mag}$ =0.013nC/sec.

From equation 5.2, one may write the following two equations for T1 and M1, respectively:

$$\frac{Q_{n\gamma}^{TE}}{A_{TE}} = D_{\gamma} + (\frac{B}{A})_{TE} D_n \qquad (5.7)$$

$$\frac{Q_{n,\gamma}^{Mag}}{A_{mag}} = D_{\gamma} + (\frac{B}{A})_{mag} D_n \qquad (5.8)$$

A_{TE} and A_{mag} were obtained from gamma-ray calibration and the results are shown in Tables 5.1 and 5.2. According to the Monte Carlo calculation, which will be introduced in the next section, the average energy of neutrons is around 2 MeV. According to Fig. 5.5, the values of $(\frac{B}{A})_{TE}$ and $(\frac{B}{A})_{mag}$ for 2-MeV neutrons are 0.97 and 0.025, respectively. Attix [86] also obtained similar results for the tissue equivalent ion chamber for neutrons with energies around 2 MeV. By substituting the numerical values into equations (5.8) and (5.9), one obtains

$$\frac{0.019\ nC/\sec}{0.01567\ nC/cGy} = 1.2125\ \ cGy/\sec = D_\gamma + 0.97 D_n$$

and

$$\frac{0.013\ nC/\sec}{0.0182\ nC/cGy} = 0.7142\ \ cGy/\sec = D_\gamma + 0.025 D_n$$

One may then solve the above two equations and obtain D_n and D_γ as follows:

$$D_n = 0.527\ cGy/\sec = 0.316 Gy/\min$$

and

$$D_\gamma = 0.7063\ cGy/\sec = 0.423 Gy/\min$$

The neutron-to-gamma ray dose ratio is, therefore, 0.747.

5.5 The Monte Carlo Calculations

To further increase the confidence of the measured neutron and gamma-ray dose components and to obtain the neutron energy spectrum (required for estimating F_1, F_2, and F_3 of the cell survival model), both the neutron absorbed dose (approximated by kerma) and the neutron energy spectrum were calculated using a Monte Carlo N-particle transport code, MCNP5 [88]. MCNP5 is a general-purpose time-dependent Monte Carlo transport code that can be used for neutron, photon and /or electron transport, including the capability to calculate eigenvalues for critical systems. The transport of particles is based on tabulated cross-section data. The code features a geometric language for specifying complex three-dimensional configurations of materials, including a system for defining portions of geometry and using them in repeated structures and lattices. In addition to the effective geometry syntax, the code also offers the ability to define very general sources, a full set of tally options, an extensive collection of variance reduction techniques and an extensive collection of cross-section data.

MCNP5 was selected to perform the calculations because it is extensively benchmarked and well accepted by the international community. The neutron spectrum was obtained by using a fine-interval energy-binned fluence tally. The details of the method used to calculate the neutron spectrum is described in the following section.

5.5.1 MCNP Modeling

The University of Maryland Training Reactor (MUTR) was modeled in MCNP5 to determine the neutron spectrum inside the beam insert at the west beam tube. The reactor was modeled in great detail. Minor components which would have little impact on the neutron spectrum were neglected in the model. The components that were

neglected consisted of items such as the lower fuel grid assembly, upper fuel grid assembly, drive motor actuators and tie rods, fission chamber internal components, and several other components that are in the reactor tank proper. All other components that comprise of the fuel rod assembly, consisting of the fuel meat, the zirconium hydride moderating rod, graphite plugs, as well as the cladding and fuel nipples were modeled in the "as built" fashion. All of the major components that comprise the core proper were modeled in a similar fashion. A picture of the core at the midplane of the beam port is shown in Fig. 5.6.

The MCNP5 model was run using the k-code module. In this module, the computer calculates k_{eff} while maintaining the correct multiplication for the fuel. The core conditions were modeled exactly as they were during the irradiations. These operating conditions consisted of components such as tank coolant temperature, fuel temperature, and control rod positions for all three control rods. The built-in temperature broadening feature (tmp card) was used. The built-in feature only corrects the 1/v cross section region of the impacted materials. This, however, is an acceptable answer because the MUTR is a thermal reactor. The control rod positions were taken as percent removed from the core (this is Maryland's standard reporting method). This percent removed is based on of the centerline of the control rod to the fuel rod. They were run out to the dimensions taken from the operating log book for the experiment. The time selected for the run was 1 hour, the approximate time of the measurements. Due to the small mean free path of fission neutrons in water and the small volume of the beam insert, the probability for a source fission neutron (starting in the core) to arrive at the beam insert is extremely small. To obtain acceptable statistics in the beam port, weight windows as well as cell importances were adjusted to provide adequate variance reduction to improve run time. The model was run for 5000 active cycles at $1x10^5$ particles per cycle. The weight window generator was used during this run. The results of the MCNP run came

up with a k_{eff} 1.00871 with a standard deviation of +/- 0.00002 with an average number of neutrons per fission reaction of 2.439.

5.5.2 The MCNP Results

The reactor geometry modeled by MCNP is in shown in Fig. 5.6.

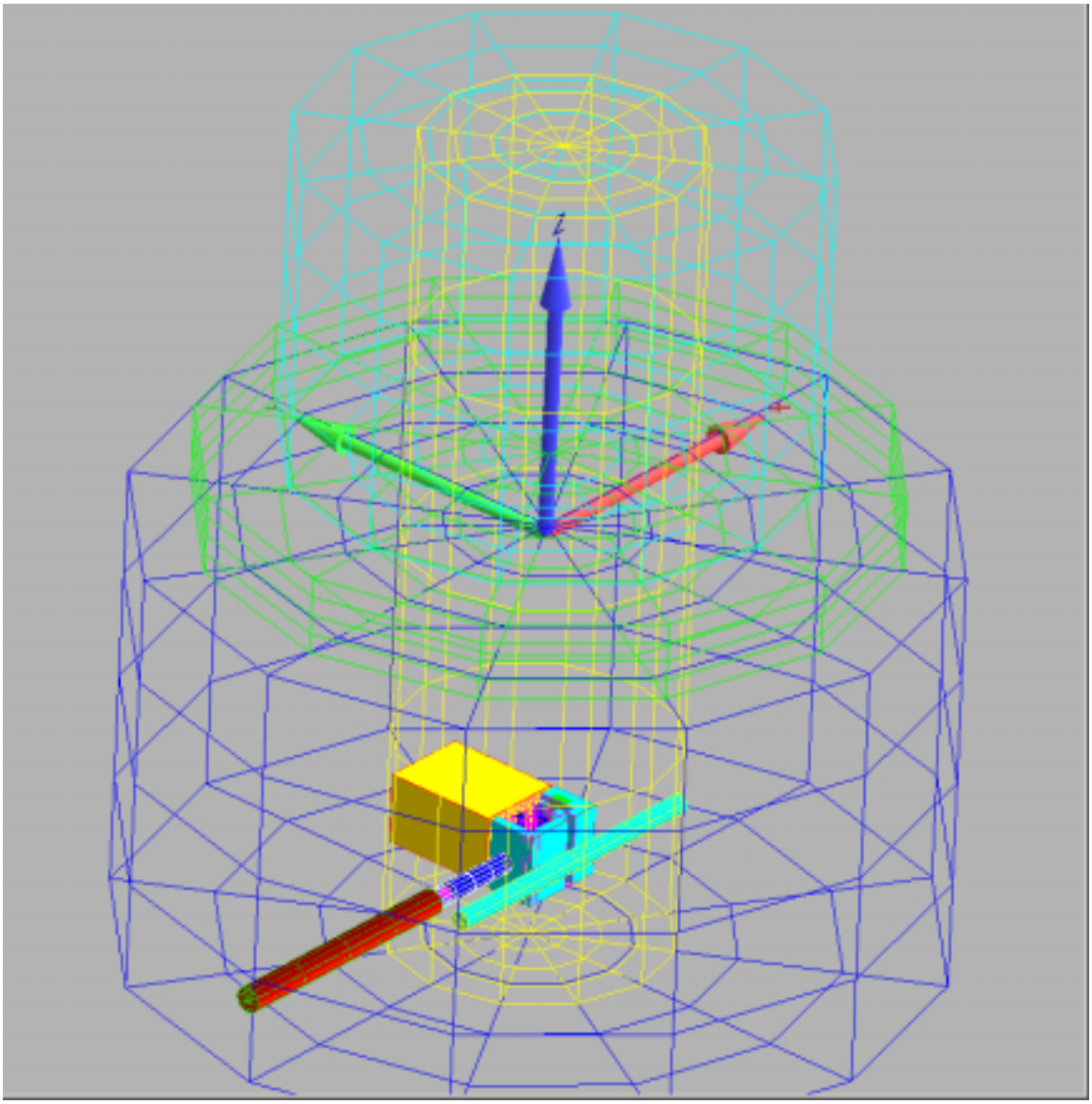

Fig 5.6 Three dimensional geometry of the MUTR modeled by MCNP

Because the neutron fluence calculated by MCNP5 is normalized to one source neutron, to obtain the absolute neutron fluence rate one must know the source neutron production rate. The neutron production rate for a 250-kW reactor can be calculated by the following equation[89]

$$N = X \times 250 \times \nu \tag{5.9}$$

Where X is the fission rate per kilowatt of power, and ν is the average number of neutrons per fission.

Using a mean value of 190 MeV per fission, the fission rate per kW of power is calculated as follows:

$$1\,kW = 10^3 \frac{Joule}{\sec} \times 6.24 \times 10^{12} \frac{MeV}{Joule} \times \frac{fiss}{190\,MeV} \times \frac{\sec}{X\ fiss},$$

which gives

$$X = 3.3 \times 10^{13} \frac{fiss}{s} \text{ per } kW$$

If one uses 2.42 for ν, then equation 5.11 would give a neutron production rate (from a 250-kW reactor) of 1.997×10^{16} neutrons/sec. The absolute neutron fluence rate at the beam insert can then be calculated as

$$\Phi = N \times P \tag{5.10}$$

Where N is the neutron n from 250 kW fission reactor, and P is the normalized neutron fluence obtained from MCNP5. The neutron spectrum calculated by MCNP5 is shown in Fig. 5.7

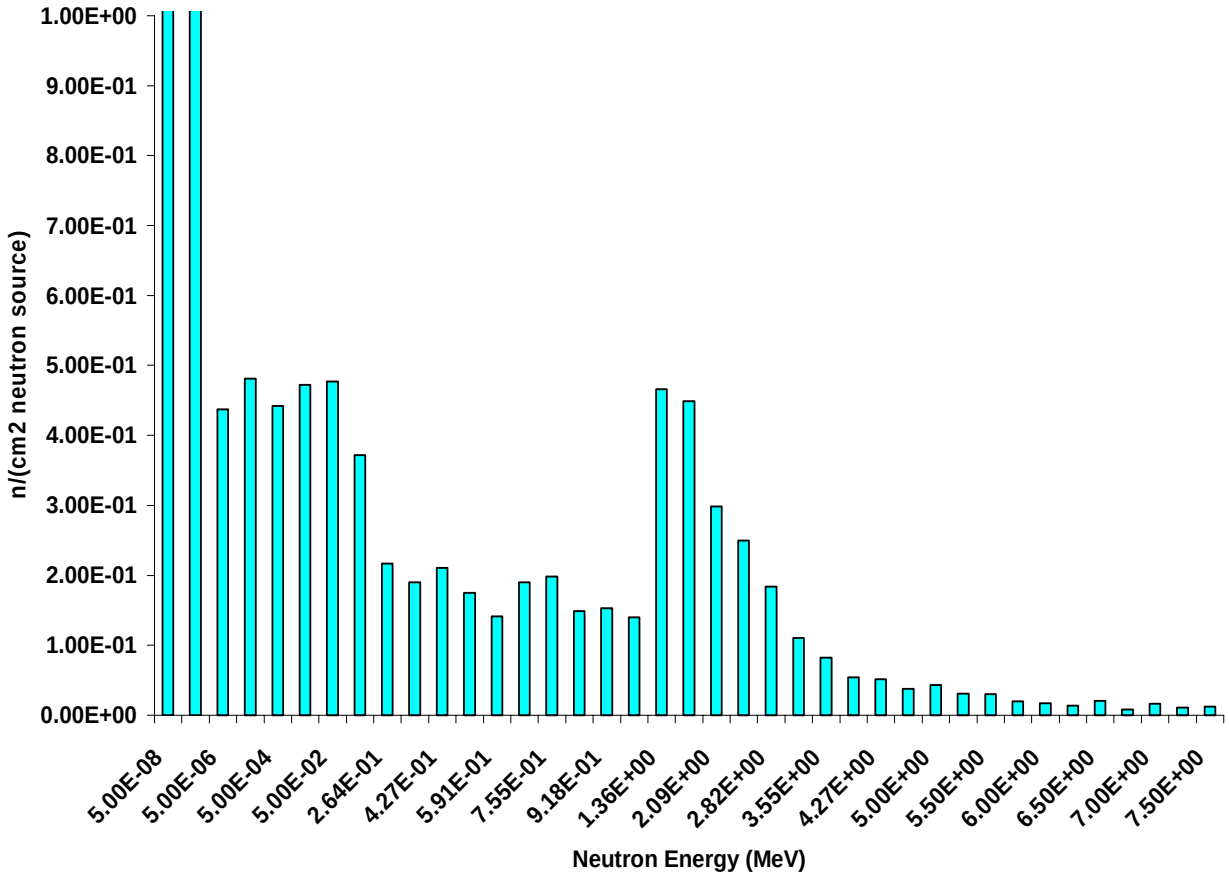

Figure 5.7 Fission neutron spectrum

The neutron absorbed dose at the beam insert was obtained by using the f6 tally in MCNP5. The f6 tally actually calculates neutron kerma (as an approximation to the absorbed dose) using the following formula[86]

$$K = \sum_i \Phi_i F_{ni} \tag{5.11}$$

Where Φ_i is the neutron fluence for the i^{th} energy bin F_{ni} is the corresponding fluence-to-kerma conversion factor. The neutron dose (or kerma) vs neutron energy obtained by MCNP5 at the beam insert is shown in Fig. 5.8.

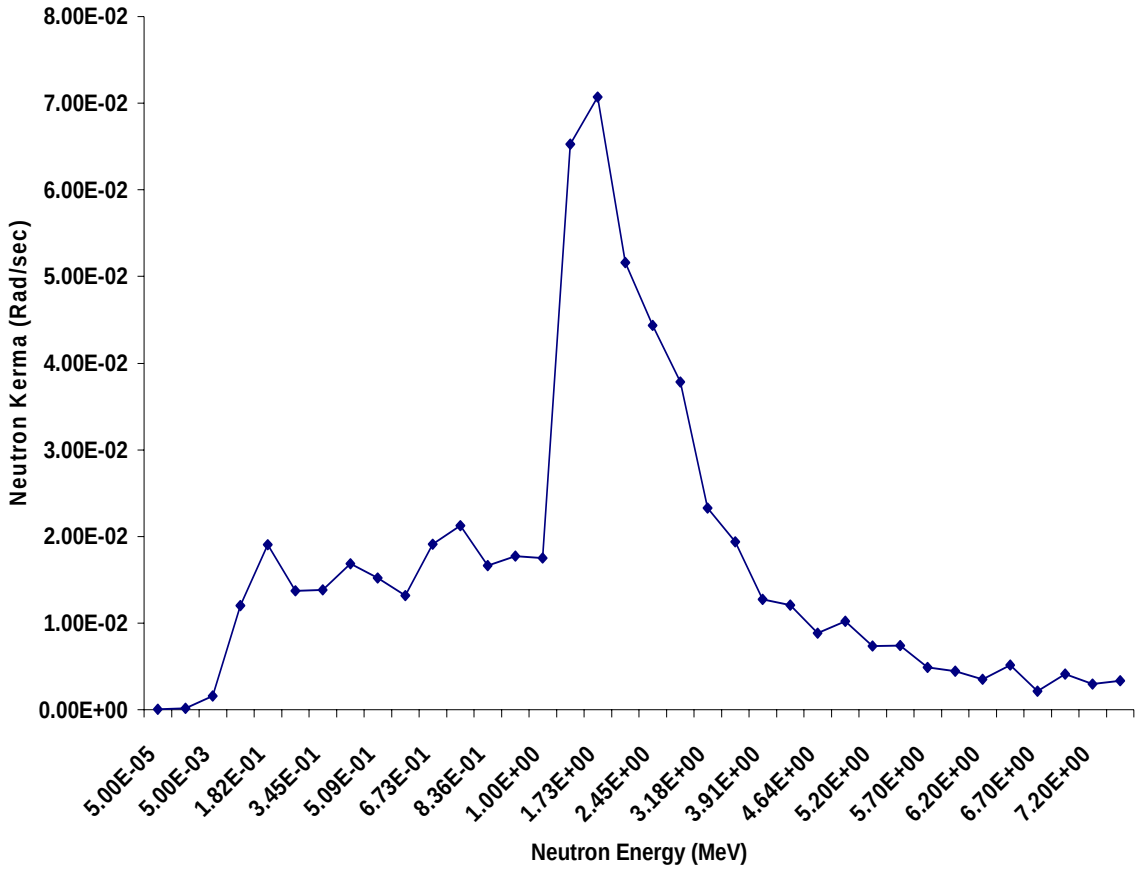

Figure 5.8 Neutron absorbed dose (or kerma) vs. neutron energy at the beam insert.

As shown, the average neutron energy is around 2 MeV, and the total fast neutron kerma at the beam insert is 0.36 Gy/min. This result compares reasonably well with the measured result of 0.316 Gy/min (see Chapter 4). The difference between the two is less than 13.9%.

The difference between the measurement and the MCNP5 calculation may be attributed to two uncertainties. The first uncertainty is associated with the values of neutron response used for the two ion chambers in the measurement. These values were not properly calibrated. Instead, they were obtained from the published data. The second uncertainty is associated with the power level used to calculate the total neutron production rate in equation 5.9.

CHAPTER 6

CELL SURVIVAL EXPERIMENT AND RESULTS

This chapter discusses the cell culture techniques, describes the V-79 cell survival experiments, and then presents the experimental results.

6.1 Cell Culture Techniques

The cell line used to conduct the cell experiment is V-79-4, which is originated from the lung tissue of a young male Chinese hamster. It has a very high plating efficiency (80%-90%) and a cell-cycle time of 12 to 14 hours. The complete growth medium is Dulbecco's modified Eagle's medium with 4 mM L-glutamine adjusted to contain 1.5g/L sodium bicarbonate with 4.5g/L glucose; 10% fetal bovine serum and 1% penicillin/Streptomycin. The V-79 cells were planted in the dishes with complete growth medium and incubated inside the Water Jacketed CO_2 Incubator (ThermoElectron Model 3110 series). The temperature of the incubator was kept at 37°C and the concentration of the CO_2 was kept at 5%.

6.1.1 Subculture

For a typical in-vitro cell survival experiment, one must first prepare a large number of cell flasks (or dishes) that contain healthy cells. Since cells quickly die as they approach full confluence in a dish, one must split (or reseed) the cells on a continuous basis. To split the cell, one first removes the medium and rinses the cell layer with 0.25%

trypsin solution, adds 1 ml trypsin-EDTA solution to the disk and then puts it back into the incubator for 1-2 minutes. One then watches the cells under an inverted microscope to observe if the cell layer is detached from the bottom of the dish. As soon as the cells are detached, one adds 6 ml of complete growth medium and then gently aspirates the cells-in-suspension with an appropriate pipettor. Finally, one adds appropriate aliquots of the cells-in-suspension to new culture disks and places them back in the incubator for continuous growth.

6.1.2 Plating Efficiency

When cells are plated out with low cell densities (2-50 cells/cm^2), they grow as discrete colonies. The planting efficiency (PE) is calculated as the following

$$PE = \frac{Number\ of\ colonies\ formed}{Number\ of\ cells\ seeded} \times 100 \qquad (6.1)$$

The PE is different for different cell lines. Generally the PE for V-79 cells is around 80-90%. But the values vary slightly among different experiments.

6.1.3 Cell and Cell Colony Counting

The number of cells planted in each dish was counted with the hemocytometer under the inverted microscope. The number of colonies formed in each dish was counted manually with a threshold of 50 or more cells per colony. That is, a colony size that is smaller than 50 cells was discarded. As far as the procedure goes, one first removes and discards the medium, rinses the monolayer with PBS, discards the rinse and adds 10 ml methanol, and then leaves it for 10 minutes. One then discards the methanol, adds 10 ml

of crystal violet (i.e. the stain) per 75cm^2 and leaves it for 10 minutes. Finally, one discards the stain, rinses the dish, and waits for the dish to dry. The dish with the colonies is then ready to be counted.

The cell culture technique is also described in Figure 6.1, and the picture of cell colonies formed is shown in Fig. 6.2 .

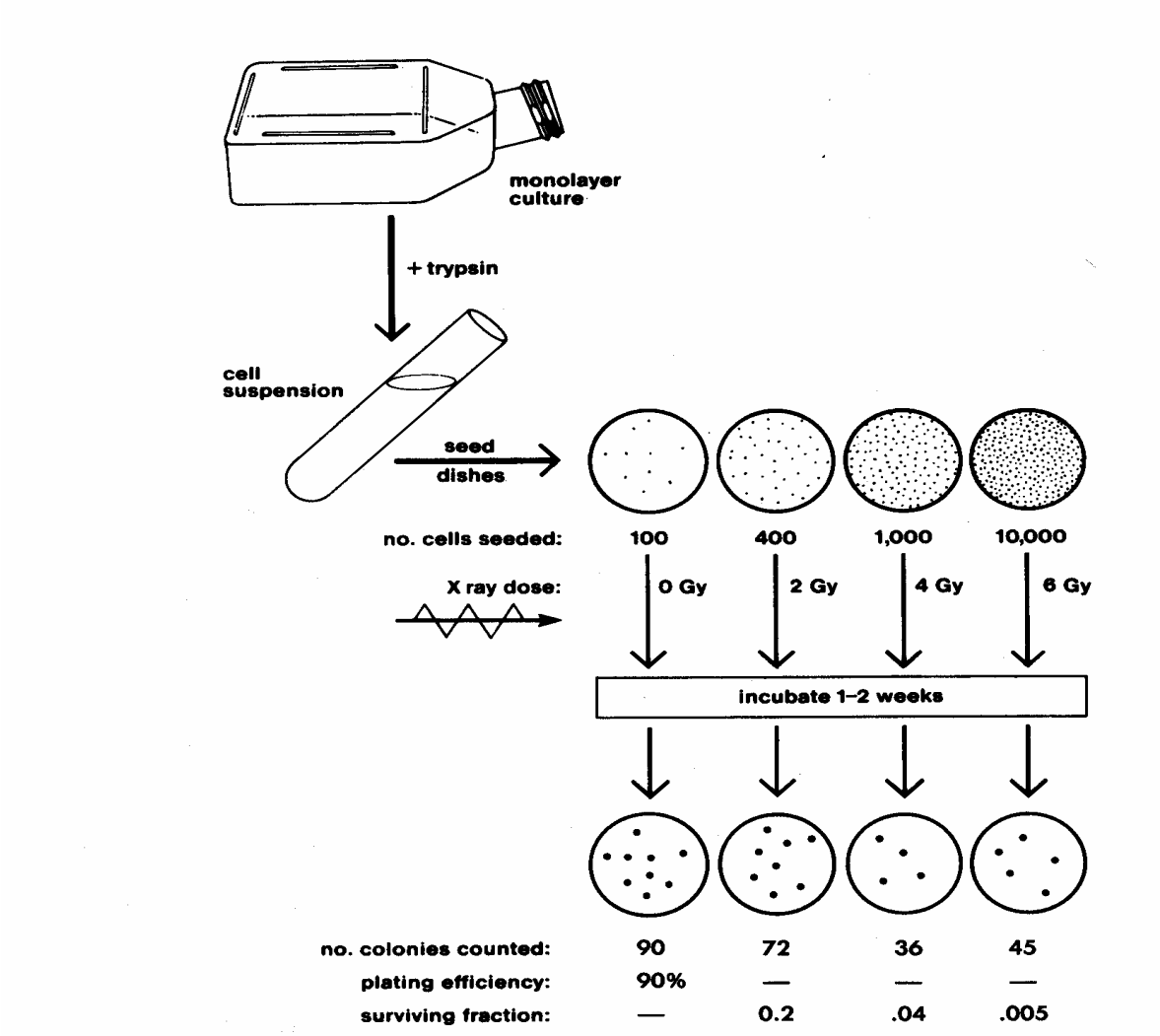

Figure 6.1: Cell culture technique for subculture and cell colony

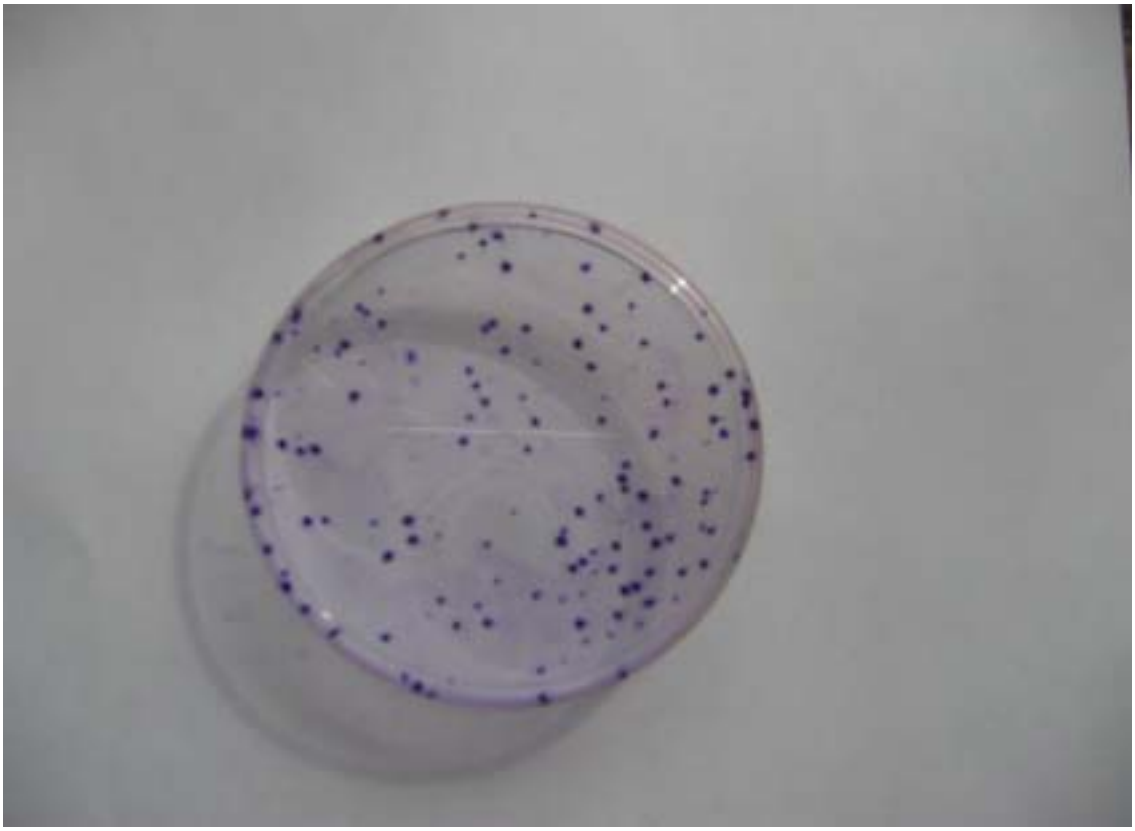

Figure 6.2: The V-79 cell colonies

6.2 Cell Irradiation

As discussed in Chapter 5, V79 cells were irradiated with ^{60}Co gamma-rays at Georgia Tech's Neely Research Center and with a mixed neutron and gamma-ray field at the MUTR. The absorbed doses to the cells were measured by placing the ion chamber M1 at the positions where cells were exposed. The dose calibration and dose measurement were described in Chapter 5. The dose rates exposed for the ^{60}Co gamma-ray experiment were 0.15 Gy/min, 0.46Gy/min, and 1.3Gy/min, respectively.

Before irradiation, cells were first transferred from round dishes (100 cm^2 in area) into the small (25 cm^2 in area) rectangle flasks and then placed back into the incubator to grow until they are ready. The most appropriate time for irradiation is when the cells reach 85%-95% confluence. The time it took to transfer the cells between the hot cell and cell culture lab in the Neely building was negligible. After the irradiation, the cells were placed back into the incubator to recover for half an hour. Different number of cells, corresponding to the various doses they received, was then reseeded into the round (100cm^2 in area) dishes. Finally, the round dishes were placed back into the incubator for about 7-10 days to allow cells to grow into colonies.

The above procedure was also followed in the irradiation experiment conducted at the MUTR. The only difference involved in the MUTR experiment was the dose measurement. As described in Chapter 5, the neutron and gamma-ray doses were measured by placing both ion chambers T1 and M1 at the cell irradiation position inside the beam insert. The flask was transferred to the cell irradiation position where the largest neutron-to-gamma dose ratio is the highest (see Fig. 6.3). The neutron dose rate during irradiation was measured to be 0.316 Gy/min and the gamma-ray dose rate was 0.423 Gy/min. The time it took to transfer the cells from the fission reactor to the cell lab was also negligible.

Figure 6.3 The beam insert with the flask inside

6.3 Experimental Results

The cell survival curves for the V79 cells resulting from the ^{60}Co gamma-ray experiment are shown in Fig. 6.4.

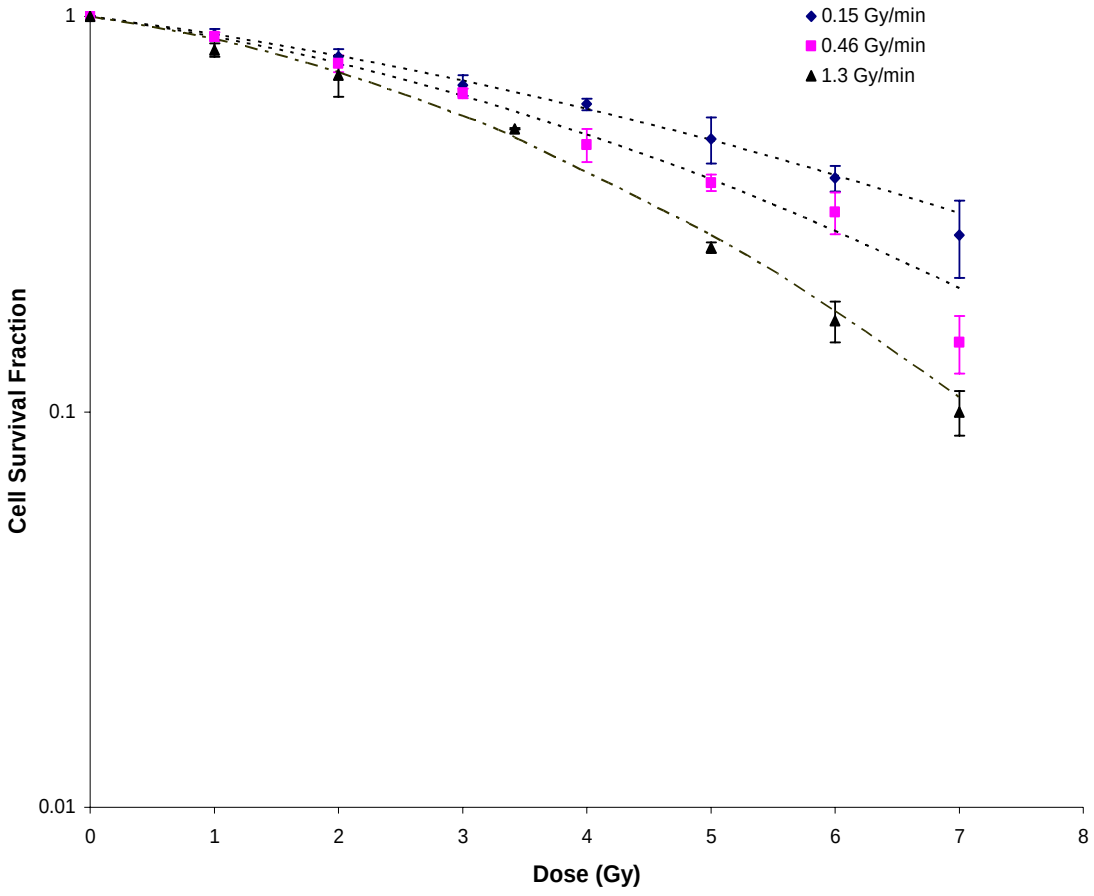

Figure 6.4 The cell survival curves for V79 cells irradiated with ^{60}Co gamma rays of various dose rate.

The cell survival curves for the V79 cells resulting from the MUTR experiment are shown in Fig. 6.5.

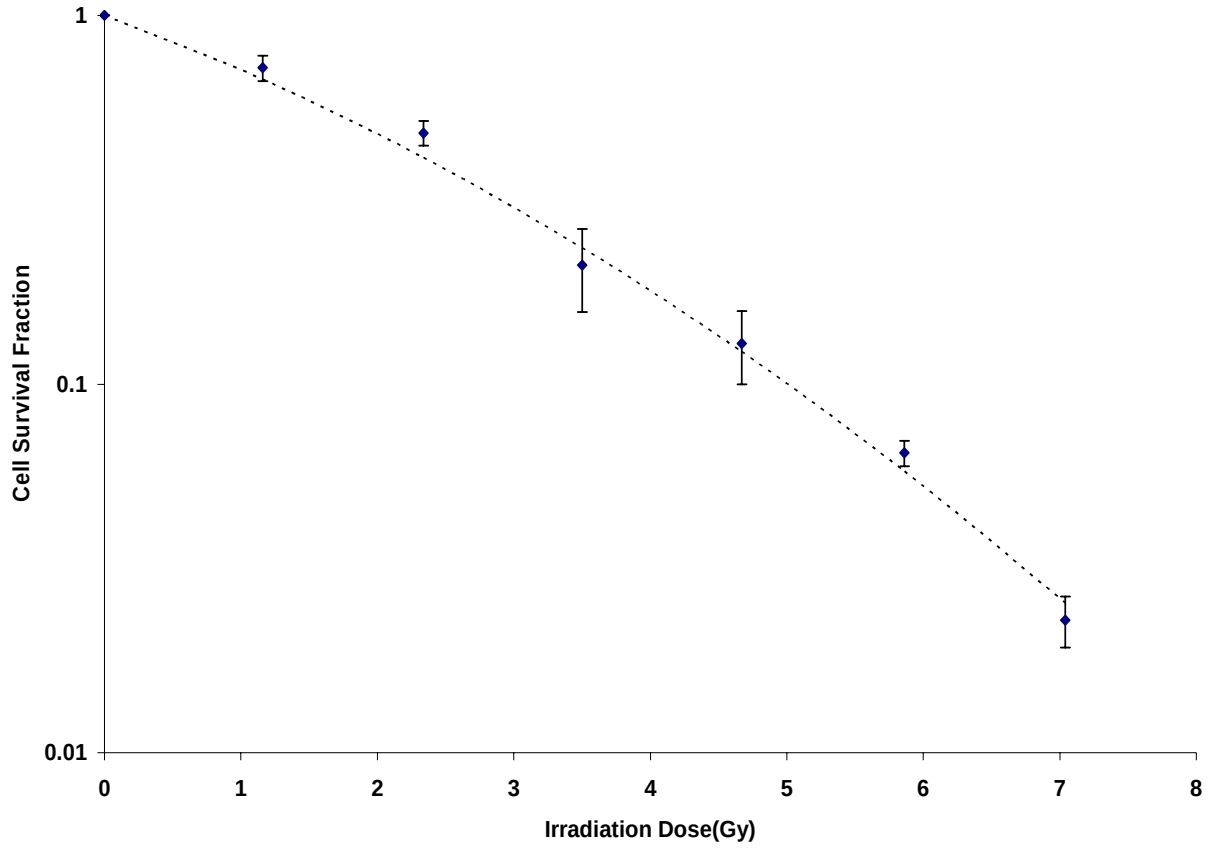

Figure 6.5 The cell survival curves for V79 cells irradiated with the mixed field of neutrons and gamma rays inside the MUTR west beam tube insert.

6.4 Validation of the New Cell Survival Model with the Experimental Results

By curve-fitting the cell survival curves of the ^{60}Co gamma-ray irradiation with the linear quadratic formula, one may derive the values of α and β. The results are shown in Table 6.1

Table 6.1 The values α and β of survival curves of V79 cells irradiated with ^{60}Co gamma rays.

	α	β
0.15 Gy/min Co-60 gamma rays	0.095	0.0098
0.46 Gy/min Co-60 gamma rays	0.1	0.018
1.3 Gy/min Co-60 gamma rays	0.1	0.03

The three physical parameters, F_1, F_2, and F_3, for ^{60}Co gamma rays are listed in Table 4.1. To obtain the values for the three biological parameters r_1, r_2 and r_3, two different cell survival curves (one for low-LET and one for high-LET) were needed as described in Chapter 4. Since the cell survival curve for fission neutrons was not available, the survival curve for 4-MeV alpha particles was used instead. This is because the slope of the survival curve for 4-MeV alpha particles is quite similar to that for the fission neutrons. The results are shown in Table 6.2.

Table 6.2 The values of r_1, r_2 and r_3 obtained from the survival curves of V79 cells irradiated with ^{60}Co gamma rays of various dose rates.

	r_1	r_2	r_3
0.15 Gy/min Co-60 gamma rays	7.78E+05	1.37E+04	3.83E+05
0.46 Gy/min Co-60 gamma rays	8.21E+05	1.22E+04	7.03E+05
1.3 Gy/min Co-60 gamma rays	8.21E+05	1.22E+04	1.17E+06

Table 6.2 shows that the values of r_1 and r_2 fluctuate very little with various dose rates. This is expected for the facts that r_1 and r_2 correspond to the routes 1 and 2, which are dominated by single track effect and irreparable lesions, and that changing the dose rate does not affect the values of r_1 and r_2. These results also agree well with the published data. The fact that r_3 varies as a function of dose rate is also consistent with the new model because r_3 corresponds to route 3 and it is dependent on the cell repair rate. For example, for the very low dose rate case (i.e. 0.15 Gy/min), some of the cells will be repaired during the fast phase repair period, and the value of r_3 is, therefore, smaller than those of the high does rate cases.

CHAPTER 7

APPLICATION OF THE NEW MODEL TO RADIATION THERAPY

Due to the recent development of a new generation high-activity miniature ^{252}Cf source [90], there is a renewed interest in ^{252}Cf brachytherapy (CBT) for treating a variety of radioresistant cancers, including cancers of the head and neck, cervical cancer, prostate cancer, melanoma, sarcoma, and malignant glioma. Numerous experimental studies have been conducted on *RBE* of ^{252}Cf neutrons, and a large deviation in the results was noted [91-92]. The deviation was largely attributable to the various absorbed doses, dose rates, and biological end points used in the experiments. In addition, the RBE was obtained based on the assumption that there are no interactions between neutron and gamma-ray lesions. However, cell survival experiments clearly show that synergistic effects do exist between x-ray and neutron damages and between x-ray and α-particle damages. [93-95].

In this chapter, a cell survival formula for mixed high- and low-LET irradiation is derived and the application using this new formula to predict the synergistic effect for mixed high- and low-LET irradiation is introduced. Since no high-dose-rate ^{252}Cf neutron source was available for this study, we used the cell survival data obtained with the mixed field of fission neutrons and gamma at the MUTR to illustrate the synergistic effect. In addition, the mixed-field cell survival data obtained at MUTR is also used to extract the RBE values for fission neutrons.

7.1 Computational Method for Mixed Field Irradiation

Studies have clearly shown that the synergistic effect does exist when cells are exposed to a mixed field of high- and low-LET particles. The new cell survival model described in Chapter 3 can be used to successfully predict the cell survival fraction for the mixed field irradiation.

To derive the cell survival fraction for mixed field high-LET and low-LET irradiation, one simply replaces the parameters in equation (3.12) with the mixed field parameters and the logarithm of the cell survival fraction for a mixed field irradiation can be expressed as

$$-\ln(S_{HL}) = \alpha_{HL} D_{HL} + \beta_{HL} D_{HL}^2 = \left[r_1 (F_1)_{HL} + r_2 (F_2)_{HL}\right] D_{HL} + r_3 (F_3)_{HL}^2 D_{HL}^2 \qquad (7.1)$$

where the subscript *HL* stands for the mixed field of high- and low-LET particles, and, accordingly,

$$D_{HL} = D_H + D_L \ , \qquad (7.2)$$

$$(F_1)_{HL} = \frac{(F_1)_H D_H + (F_1)_L D_L}{D_H + D_L}, \qquad (7.3)$$

$$(F_2)_{HL} = \frac{(F_2)_H D_H + (F_2)_L D_L}{D_H + D_L}, \qquad (7.4)$$

And

$$(F_3)_{HL} = \frac{(F_3)_H + (F_3)_L}{D_H + D_L} \tag{7.5}$$

Substituting Eqs. (7.2), (7.3), (7.4) and (7.5) into Eq. (7.1), one obtains

$$\begin{aligned} -\ln(S_{HL}) &= [r_1(F_1)_H + r_2(F_2)_H]D_H + [r_1(F_1)_L + r_2(F_2)_L]D_L + \\ &\quad + r_3\left[(F_3)_H^2 D_H{}^2 + (F_3)_L^2 D_L{}^2 + 2(F_3)_H (F_3)_L D_H D_L\right] \\ &= \alpha_H D_H + \beta_H D_H{}^2 + \alpha_L D_L + \beta_L D_L{}^2 + \beta_{HL} D_H D_L \end{aligned} \tag{7.6}$$

where

$$\beta_{HL} = 2\, r_3\, (F_3)_H\, (F_3)_L \tag{7.7}$$

which represents the contribution from the interaction between the lesions caused by the high-LET particles and that caused by the low-LET particles.

7.2 Calculated Cell Survival Fraction for Mixed n-γ Irradiation

The cell survival fraction irradiated with a mixed field of fission neutrons and gamma-rays can be calculated by the new model according to equation (7.6). Since the pure neutron irradiation is not available for this cell experiment, the neutron cell survival fraction was calculated using the new model. The cell survival curve irradiated with gamma-rays was obtained from cell experiments.

7.2.1 Calculated Cell survival Fraction for Neutron Irradiation

The survival fraction of cells irradiated with neutrons can be calculated by the new model described in Chapter 3. To do so, one must first obtain the spectra of recoil protons and then calculate the nanodosimetry quantities, F_1, F_2 and F_3. For a neutron field, the recoil proton spectrum can be calculated as

$$S(E_p)dE_p = \int_{E_p}^{E_n} S(E_p, E_n)\sum_s (E_n)\phi(E_n)dE_n dE_p \tag{7.8}$$

where $S(E_{p,}E_n)dE_p$ is the proton spectrum for neutrons with energy E_n, and $\sum_s (E_n)$ and $\phi(E_n)$ are, respectively, the macroscopic scattering cross section and the fluence rate for neutrons with energies between E_n and $E_n + dE_n$.

The neutron spectrum $\phi(E_n)$ at the MUTR cell irradiation facility was calculated by MCNP5 and has been discussed in Chapter 5. The proton spectrum thus obtained with equation (7.8) is shown in Fig. 7.1. The three physical parameters F_1, F_2 and F_3 can then be calculated using the recoil proton spectrum and the published computational data for 5-nm and 25-nm targets [83-85]. The values for these three parameters calculated are: $F_1 = 6.6\times10^{-9}$, $F_2 = 1.7\times10^{-7}$ and $F_3 = 1.43\times10^{-6}$.

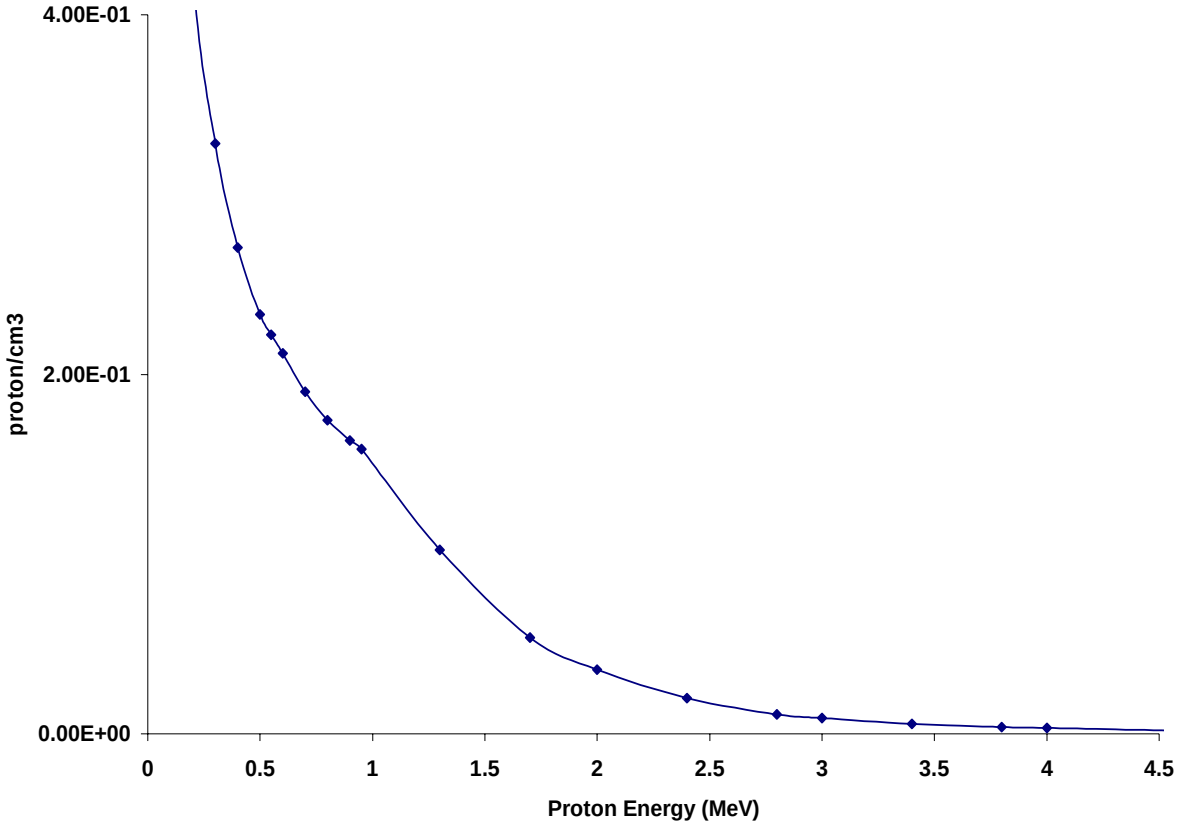

Figure 7.1. Recoil proton spectrum at the MUTR beam insert.

The next step was to calculate α and β using equations 3.13 and 3.14 , i.e. $\alpha = r_1 F_1 + r_2 F_2$ and $\beta = r_3 F_3^{\,2}$. We chose $r_1 = 7.84 \times 10^5$ and $r_2 = 1.96 \times 10^4$, which were suggested in Chapter 4. We chose $r_3 = 1.41 \times 10^6$, which corresponds to the averaged value for high dose rate irradiation. This is because for neutron irradiation, the cell repair will be negligible especially when the irradiation time is short. The cell survival fraction (i.e. curve) for neuron irradiation thus calculated is shown in Fig. 7.2.

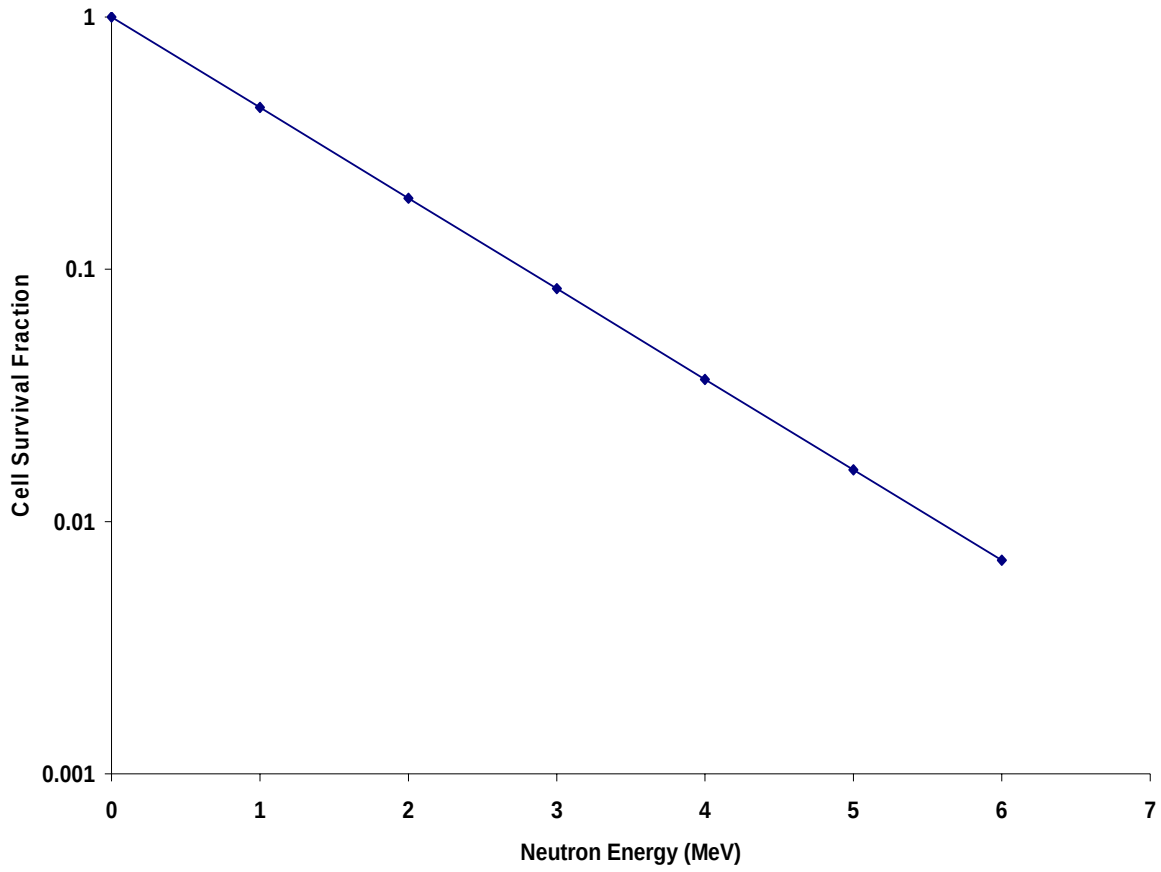

Figure 7.2. The calculated survival curve for V-79 cells irradiated with fission neutrons.

7.2.2 Calculated Cell Survival Fraction for Mixed n-γ Irradiation

The cell survival fraction for mixed n-γ irradiation can be calculated using equation (7.6), i.e. $-\ln(S_{n\gamma}) = \alpha_n D_n + \beta_n D_n^{\,2} + \alpha_\gamma D_\gamma + \beta_\gamma D_\gamma^{\,2} + \beta_{n\gamma} D_n D\gamma$. The values for α_n and β_n were determined to be 8.27×10^{-1} and 2.87×10^{-6}, respectively, and they were obtained from the cell survival curve shown in Fig. 7.2. The values for α_γ and β_γ were determined to be 0.1 and 0.018, respectively, and they were obtained from the cell survival curves shown in Fig. 6.4 or Table 6.1. The value of $\beta_{n\gamma}$ was calculated using equation (7.7), i.e. $\beta_{n\gamma} = 2\, r_3 \,(F_3)_n \,(F_3)_\gamma = 5.63\times10^{-2}$. The cell survival curve for mixed n-γ irradiation thus calculated is shown in Fig. 7.3. Also shown in this figure are the corresponding neutron-only and gamma-ray-only cell survival curves. The gamma-ray-only curve was based on the ^{60}Co gamma-ray experiment with 0.46 Gy/min dose rate.

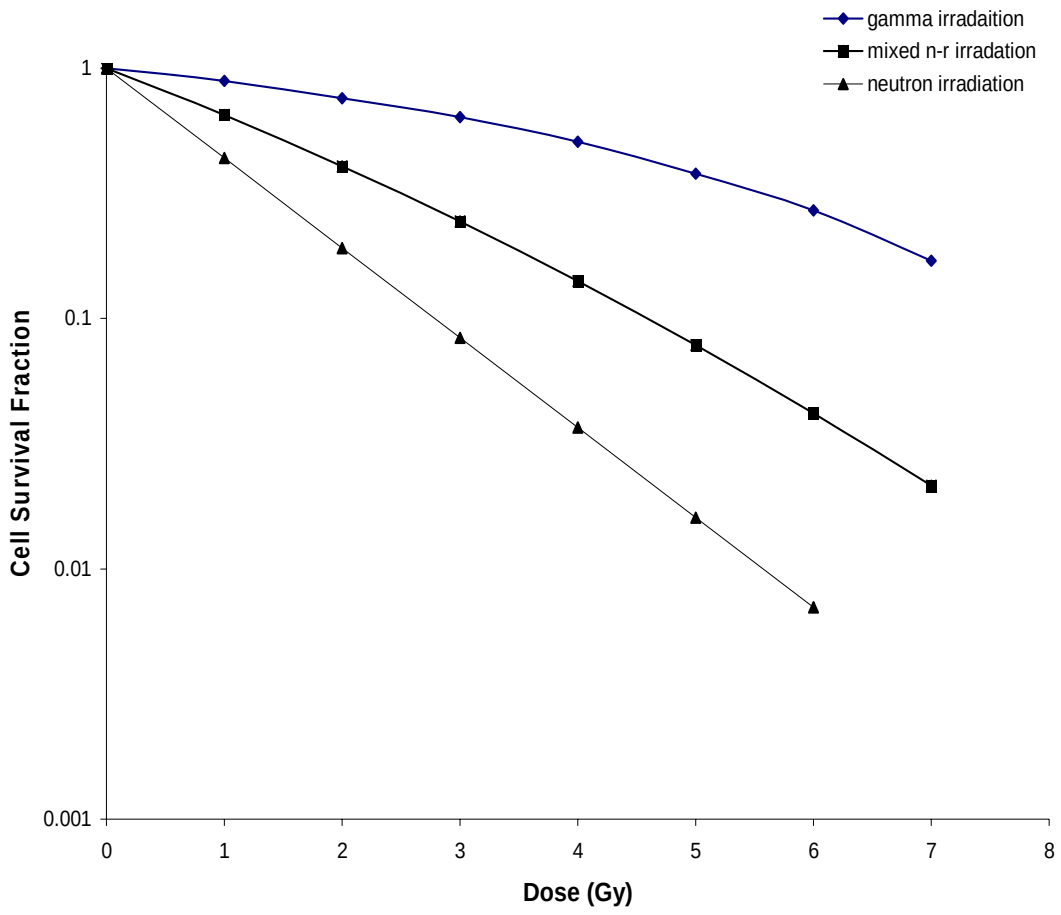

Figure 7.3. V-79 Cell survival curves for the mixed neutron and gamma rays irradiation.

7.2.3 Comparison Between the Experimental results and the Computational Results

The cell survival curve for mixed n-γ irradiation obtained from cell experiment is shown in Fig. 7.4. For comparison, the two computationally derived survival curves (i.e. those with and without the synergistic term) are also included in Fig. 7.4. In general, the experimentally obtained cell survival fractions are slightly higher than those predicted by the new cell survival model especially for the low dose data.

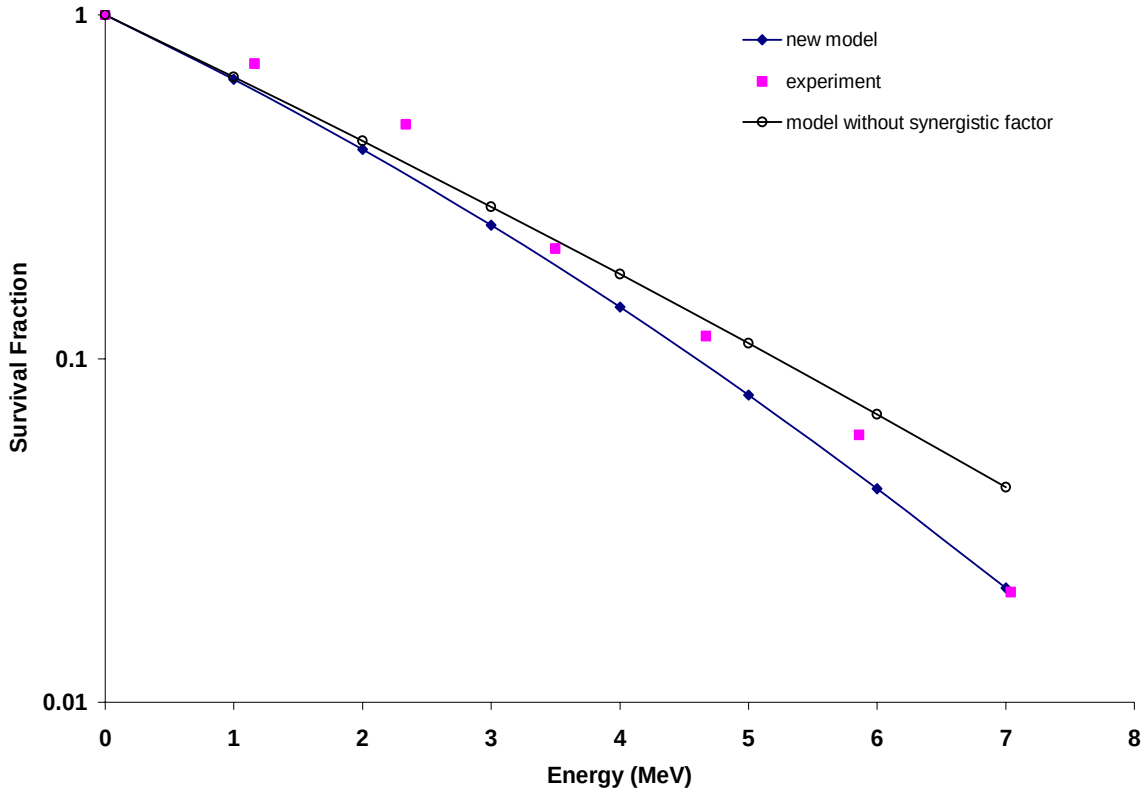

Figure 7.4 Cell survival curves for mixed n-γ irradiation.

The difference between these two cell survival curves may be attributed to three factors. The first one is the uncertainty associated with the parameters used in the new cell survival model. That is, these parameters were based on the two cell survival curves, the neutron-only cell survival curve and the gamma-ray-only cell survival curve. The uncertainty mainly comes from the neutron-only cell survival curve because it was based on calculations instead of actual experimental results. The second factor is the uncertainty associated with the three biological parameters, which have already been discussed in Chapter 4. The third factor is the uncertainty associated with cell counting.

The synergistic effect shown in Fig. 7.4 can be more explicitly illustrated as follows: For typical ^{252}Cf brachytherapy doses of D_n = 4 Gy and D_γ = 2 Gy, the new cell survival model predicts a value of 0.6372 for the synergistic term $\beta_{n\gamma} D_n D_\gamma$, which translates to an additional 36.3% of cell killing.

7.2.4 Relative Biological Effectiveness of Fission Neutrons

As mentioned in the beginning of this chapter, the accuracy of the relative-biological-effectiveness (*RBE*) value for fission neutrons has been an issue for the ^{252}Cf-based brachytherapy. By definition, the neutron *RBE* is obtained with the following equation [96]:

$$RBE = \frac{D_\gamma}{D_n} \tag{7.9}$$

where D_γ is the dose that is needed for a low-LET reference source (i.e. a 250 kVp x-ray or a ^{60}Co gamma-ray source) to produce a given biological effect, and D_n is the dose that

is needed for the test radiation (i.e. the fission neutrons in this study) to produce the same biological effect.

To be consistent with the conventional radiation therapy where dose is delivered in a multi-fraction scheme with 2 Gy per fraction, the *RBE* values for fission neutrons, $(RBE)_n$, were obtained by comparing the survival curve of a multi-fraction ^{60}Co γ-ray (as the low-LET reference source) with either the calculated fission neutron survival curve shown in Fig. 7.2, or the experimentally obtained mixed n+γ survival curve shown in Fig. 7.4. The survival curve of the multi-fraction ^{60}Co γ-ray were artificially generated by using the high-dose-rate (i.e. 1.3 Gy/min) data and the following formula:

$$S_i = (S_1)^i \tag{7.10}$$

where S_1 is the cell survival fraction after a single fraction of 2 Gy, and S_i is the cell survival fraction after i fractions with 2 Gy per fraction. Figure 7.5 shows this "artificial" multi-fraction cell survival curve, together with the other two survival curves – i.e. the fission neutron survival curve and the mixed n+γ survival curve.

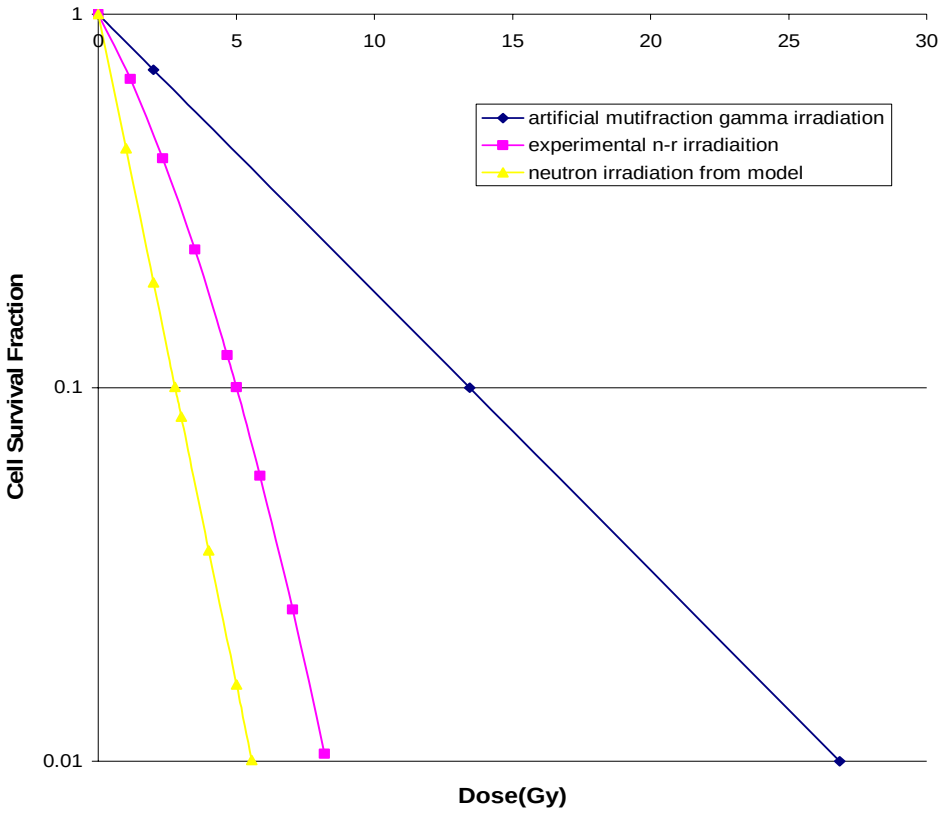

Figure 7.5 The V-79 cell survival curves used for RBE calculation

By evaluating the corresponding dose components of the survival curve of the multi-fraction ^{60}Co γ-ray and of the calculated fission neutron survival curve for survival fractions of 10% and 1% and by using equation (7.9), one may easily obtain the values of $(RBE)_n$. The dose components and the $(RBE)_n$ values thus obtained are shown in Table 7.1. The fact that the $(RBE)_n$ values are the same for survival fractions of 10% and 1% is because both survival curves are straight lines, indicating that lesion interactions (i.e. the quadratic term) play no role in cell death in both curves.

Table 7.1. The dose components and the $(RBE)_n$ values obtained from the calculated fission neutron survival curve.

Biological End Point	D_n	D_γ	$(RBE)_n$
10% cell survival fraction	2.78	13.45	4.83
1% cell survival fraction	5.56	26.89	4.83

To obtain $(RBE)_n$ via the mixed n+γ survival curve, one evaluates dose components for survival fractions of 10% and 1% using the following equation:

$$(RBE)_n \times D_{n-mix} + D_{\gamma-mix} = D_\gamma \qquad (7.11)$$

where $D_{n\text{-}mix}$ and $D_{\gamma\text{-}mix}$ are the neutron dose and gamma dose, respectively, and D_γ is the gamma dose corresponding to the "artificial" multi-fraction survival curve of ^{60}Co γ-ray. For example, for the case of 10% cell survival fraction, the corresponding values of $D_{n\text{-}mix}$, $D_{\gamma\text{-}mix}$, and D_γ are 2.14, 2.86, and 13.45. By substituting these values into equation (7.11), one obtains an $(RBE)_n$ of 4.95. The fact that the experimentally obtained value (i.e. 4.95) agrees well with the calculated value (i.e. 4.83) serves as an additional validation for the new cell survival model. Table 7.2 shows the dose components and the

$(RBE)_n$ values obtained for survival fractions of 10% and 1% using the mixed n+γ survival curve. It is interesting to note that the experimentally obtained $(RBE)_n$ value of 6.32 for survival fraction of 1% is significantly greater than the value of 4.95 for survival fraction of 10%. This is consistent with the finding in Section 7.2.3 in that the synergetic effect due to the interactions of neutron and gamma-ray lesions contributes to additional cell killing, and thus increasing the $(RBE)_n$ value. The $(RBE)_n$ value of 6.32 is also consistent with the value of 6.0 often used in the ^{252}Cf-based brachytherapy where the total neutron dose is around 4 Gy.

Table 7.2. The dose components and the $(RBE)_n$ values obtained from the experimentally obtained mixed n+γ survival curve.

Biological End Point	$D_{n\text{-}mix}$	$D_{\gamma\text{-}mix}$	D_γ	$(RBE)_n$
10% cell survival fraction	2.14	2.86	13.45	4.95
1% cell survival fraction	3.51	4.69	26.89	6.32

CHAPTER 8

CONCLUSIONS AND FUTURE WORK

Several conclusions can be made for this thesis. First, the new nanodosimetry-based cell survival model for mixed low- and high-LET radiation has been developed. Two specific sizes of subcellular target, 5 nm and 25 nm, were defined and several dosimetry quantities based on these two nanometer target sizes were used to develop the new model. The final expression of this new model is expressed as a linear quadratic formula, $\alpha D + \beta D^2$, where α and β are expressed by three physical quantities associated with energy deposition at nanometer scales, and the three biological quantities associated with lesion production and interaction probabilities and lesion repair rate. Second, the new survival model has been validated by using the previously published survival data of V-79 hamster cells and by conducting additional V79 cell survival experiments specifically designed for this study at the MUTR. Third, the new model has been successfully used in the ^{252}Cf-based brachytherapy to predict: (1) the synergistic effect between neutron and gamma-ray lesions, and (2) the neutron RBE.

As to the future work, several areas should be considered: First, the counting technique both for the cell number and for the colony number needs to be improved. For example, one may develop an automatic counting system to count accurately both the number of cells the number of cell colonies. Second, further validation of the new survival model should be conducted using cell lines other than V79 and comparison of the cell survival results should be made between normal cell lines and cancer cell lines. Third, the new survival model should be modified to include prediction of the number of chromosome aberrations as a function of dose and dose rate.

APPENDIX

MCNP5 INPUT FILE

```
Maryland TRIGA Rx k-code flux tally model
C ****************************************
C Cell Cards
C ****************************************
1 1 -6.53 -1       u=1  tmp=3.3694e-8      imp:n=1 $ Zirconium rod
2 2 -6 -2 1        u=1  tmp=3.3694e-8      imp:n=1 $ fuel meat
3 3 -1.3 -3        u=1  tmp=2.67915e-8     imp:n=1 $ graphite plug bottom
4 3 -1.3 -4        u=1  tmp=2.67915e-8     imp:n=1 $ graphite plug top
5 4 -8.03-5 4 3 2  u=1  tmp=2.67915e-8     imp:n=1 $ cladding no air gap
6 5 -1 -6 5        u=1  tmp=2.67915e-8     imp:n=1 $ water outside clad
7 5 -1 6           u=1  tmp=2.67915e-8     imp:n=1 $ outside of universe space
c 21 like 1        but mat=6 rho=-1.21e-3 u=3 tmp=2.67915e-8
c 22 like 2        but mat=6 rho=-1.21e-3 u=3 tmp=2.67915e-8
c 23 like 3        but mat=6 rho=-1.21e-3 u=3 tmp=2.67915e-8
c 24 like 4        but mat=6 rho=-1.21e-3 u=3 tmp=2.67915e-8
c 25 like 5        but u=3 tmp=2.67915e-8
c 26 like 6        but u=3 tmp=2.67915e-8
c 27 like 7        but u=3 tmp=2.67915e-8
21 10 -2.5 -71     imp:n=1 u=3   tmp=2.67915e-8
22 5 -1     71     imp:n=1 u=3   tmp=2.67915e-8
23 10 -2.5 -72     imp:n=1 u=14  tmp=2.67915e-8
24 5 -1     72     imp:n=1 u=14  tmp=2.67915e-8
25 10 -2.5 -73     imp:n=1 u=18  tmp=2.67915e-8
26 5 -1     73     imp:n=1 u=18  tmp=2.67915e-8
8 5 -1 -6          fill=1  u=2   imp:n=1 tmp=2.67915e-8
12 5 -1 6          u=2 imp:n=1 tmp=2.67915e-8
9 like 8 but fill=3 u=4 tmp=2.67915e-8
10 like 12 but u=4 tmp=2.67915e-8
109 like 8 but fill=14 u=20 tmp=2.67915e-8
110 like 12 but u=20 tmp=2.67915e-8
111 like 8 but fill=18 u=19 tmp=2.67915e-8
112 like 12 but u=19 tmp=2.67915e-8
113 5 -1 -6 lat=1 fill=0:1 0:1 0:0  2 2 2 4  u=16 tmp=2.67915e-8 imp:n=1
161 5 -1 -7   fill=16 u=17 tmp=2.67915e-8  imp:n=1
171 5 -1  7   u=17         tmp=2.67915e-8  imp:n=1
13 5 -1  -6   lat=1 fill=0:1 0:1 0:0   2 2 2 20 u=10 tmp=2.67915e-8 imp:n=1
61 5 -1  -7   fill=10 u=6  tmp=2.67915e-8    imp:N=1
71 5 -1   7   u=6                  tmp=2.67915e-8      imp:n=1
15 5 -1  -6    lat=1 fill=0:1 0:1 0:0   2 2 2 2 u=11 tmp=2.67915e-8 imp:n=1
62 5 -1  -7   fill=11 u=5        tmp=2.67915e-8      imp:N=1
72 5 -1   7            u=5        tmp=2.67915e-8      imp:n=1
16 5 -1  -6     lat=1 fill=0:1 0:1 0:0   2 2 19 2 u=12 tmp=2.67915e-8 imp:n=1
63 5 -1  -7    fill=12 u=7    tmp=2.67915e-8           imp:N=1
73 5 -1   7    u=7            tmp=2.67915e-8           imp:N=1
17 3 -1.3 -7   u=8            tmp=2.67915e-8           imp:n=1
18 5 -1  -7    u=9            tmp=2.67915e-8           imp:n=1
14 0  6        u=10           imp:n=1 tmp=2.67915e-8
19 5 -1  7     u=8            imp:N=1 tmp=2.67915e-8
30 like 14 but u=11 tmp=2.67915e-8
31 like 14 but u=12 tmp=2.67915e-8
33 like 19 but u=9 tmp=2.67915e-8
28 like 18 but mat=6 rho=-1.21e-3 u=13 imp:n=1 tmp=2.67915e-8
29 like 19 but u=13   tmp=2.67915e-8    imp:n=1



50 5 -1   -7  lat=1  fill=0:8 0:4 0:0
          9 9 9 9 9 5 9 9 9
          9 5 5 6 5 13 5 9 9
          9 5 5 5 5 5 5 8 9
```

```
          9 5 17 5 5 7 5 8 9
          9 5 5 5 5 5 5 9 9
               u=15   tmp=2.67915e-8                    imp:N=1
51 0   7       u=15                                     imp:N=1
52 5 -1  -8 fill=15    tmp=2.67915e-8                   imp:n=1
53 5 -1    -10 11 12 13 8 16                            imp:N=1
55 3 -1.3  -11                                          imp:n=1
56 7 -2.7  -12 14 17                                    imp:n=1
58 6 -1.21e-3  -14 15                                   imp:n=1
59 8 -11.8  -15                                         imp:n=1
57 6 -1.21e-3 -13                                       imp:n=1
60 6 -1.21e-3 -16 12 18 19 20 21                     ip:N=100
81 8 -11.8  -17                                         imp:N=100
82 7 -2.7   -18 19 20 21                                imp:N=100
83 8 -11.8  -19 20 21                                   imp:n=100
84 7 -2.7   -20 21                                      imp:N=100
85 6 -1.21e-3 -21                                       imp:n=100
86 9 -2.3      (-50:-51:-52) 10 11 12 13 14 16  imp:n=1
54 0        50 51 52 16                                 imp:N=0

C ***************************************
C Surface Cards
C ***************************************
1 rcc 0 0 0      0 0 38.1     .2285
2 rcc 0 0 0      0 0 38.1     1.74
3 rcc 0 0 -8.76  0 0 8.76     1.74
4 rcc 0 0 38.1   0 0 8.76     1.74
5 rcc 0 0 -8.811 0 0 55.722    1.791
71 rcc 0 0 36.528 0 0 43.2    1.7
72 rcc 0 0 40.338 0 0 43.2    1.7
73 rcc 0 0 35.0134 0 0 43.2   1.7
6 rpp -1.9434 1.9434  -1.9434 1.9434   -8.811 97
7 rpp -1.9434 5.829 -1.9434 5.829 -8.811 97
8 rpp -1.9433 66.6366 -1.9433 36.91 -8.811 97
9 rpp -1.9433 66.6365 -1.9433 36.1565 -8.812 96.9999
10 rcc 23 18 -48          0 0 648    106.5
50 rcc 23 18 -48          0 0 335.28 304.62
51 rcc 23 18 287.28       0 0 60.96  258.9
52 rcc 23 18 348.24       0 0 251.76 197.94
11 rpp -1.9 66 39.45 130 -8 47
12 rcc -4.4833 21.125 19.05 -79.5717 0 0 7.46125
14 rcc -5.1183 21.125 19.05 -60.7367 0 0 6.82625
15 rcc -5.1183 21.125 19.05 -7.62   0 0 6.82625
16 rcc -83.42 21.125 19.05 -200 0 0     10.08507
17 rcc -67.13 21.125 19.05 -15.24 0 0 6.12775
18 rcc -84.055 21.125 19.05 -43.815 0 0 6.76275
19 rcc -84.055 21.125 19.05 -43.815 0 0 6.11251
20 rcc -84.055 21.125 19.05 -43.815 0 0 5.08
21 rcc -84.055 21.125 19.05 -43.815 0 0 4.445
13 rcc -90 -11.46125 19.05   240 0 0 7.46125

C ***************************************
C Data Cards
C ***************************************
m2 40000 -.89813 1001 -9.92e-3 92238 -6.2e-2 92235 -1.95e-2
mt2 zr/h.62t h/zr.62t
m1 40000 -1
m3 6012 -1
mt3 grph.62t
m4 6012 -.0003 24000 -.19 26000 -.7015 25055 -.02 28000 -.1
          15031 -.00045 16000 -.0003 14000 -.0075  $ SS304 from matls.com
m5 1001 2 8016 1
mt5 lwtr.61t
```

```
m6 6000 -1.24e-5 7014 -.755268 8016 -.231781 18000 -.012827
                  $ NIST dry air (sea level
m7 13027 -.991 26000 -.008 12000 -.0009 23000 -.000015 22000 -.000015
              29000 -.00004 24000 -.00001 14000 -.00003   $ Al 1100 grade
m8 82000 -1                 $ pure lead (not actually, but who knows)
m9 1001 -.0221 6000 -.002484 8016 -.57493 11023 -.015208 12000 -.001266
         13027 -.019953 14000 -.304627 19000 -.010045 20000 -.042951
         26000 -.006435             $ NIST concrete
m10 5011 3.2 5010 .8 6000 1
f2:n 8.2
f12:n 18.2
f4:n 85
f22:n 12.2
sd2 434
sd4 2719.6678
e0 5e-8 8e-7 5e-6 5e-5 5e-4 5e-3 5e-2 1.82e-1 2.64e-1 3.45e-1 4.27e-1 5.09e-1
         5.91e-1 6.73e-1 7.55e-1 8.36e-1 9.18e-1 1 1.36 1.73 2.09 2.45 2.82
         3.18 3.55 3.91 4.27 4.64 5 5.2 5.5 5.7 6 6.2 6.5 6.7 7 7.2 7.5 7.7 8
         8.2 8.5 8.7 9 9.2 9.5 9.7 10 10.2 10.5 10.7 11 11.2 11.5 11.7 12 12.2
         12.5 12.7 13 13.2 13.5 13.7 14 14.2 14.5 14.7 15 16 17 18 19 20 50 100
c        Energy bins for dE/dF energy conversion to be conducted
c       outside the code.
mesh geom=rec origin=-300 -300 -50 kmesh 0 30i 30 600 imesh -195 10i -90 90i
         0 20i 20 300 jmesh 5 35i 40 300 ref=1e-6 1e-7 0
c      weight window mesh for variance reduction purposes
wwg 12 0 5j 0
c ssr old=8.2 new=8.2
rand gen=2 seed= 6516161565161
c using the 64 bit random number generator with a random seed
c obtained by pure luck of striking the keyboard repeatedly
c ssw 8.2 sym=2
kcode 5e5 1.0 2 422
c ksrc 31.1 26.43 20 27.3 26.29 20 19.88 26.40 20
c nps 15148787
c nonu
```

REFERENCES

[1] R. Railton, R. C. Lawson and D. Porter, "Interaction of γ-ray and neutron effects on the proliferative capacity of Chinese hamster cells," Int. J. Radiat. Biol., vol. 27(1), pp.75-82, 1975.

[2] F. Q. H. Ngo, E. A. Blakely and C. A. Tobias, "Sequential exposures of mammalian cells to low- and high-LET radiations. I. Lethal effects following X-ray and neon-ion irradiation," Radiat. Res., vol. **87**, pp. 59-78, 1981.

[3] P. D. Higgins, P. M. DeLuca, Jr. and D. W. pearson, "V79 survival following simultaneous or sequential irradiation by 15-MeV neutrons and ^{60}Co photons," Radiat. Res., vol. 95, pp. 45-56, 1983.

[4] R. Bird, M. Zaider, H. H. Rossi and E. J. Hall, "The sequential irradiation of mammalian cells with X rays and charged particles of high LET". Radiat. Res., vol. 93, pp. 444-452, 1983.

[5] M. J. Rivard, C.S. Melhus, H.D. Zinkin, "A radiobiological model for the relative biological effectiveness of high-dose-rate ^{252}Cf Brachytherapy," Radiat. Res., vol. 164, pp. 319-323, 2005.

[6] M. Zaider and H. H. Rossi, "The synergistic effect of different radiations," Radiat. Res., vol. 83, pp. 732-739, 1980.

[7] C. Streffer and W. U. Mueller, "Dose-effect relationships and general mechanisms of combined exposures," Int. J. Radiat. Biol., vol. 51, pp. 961-969, 1987.

[8] G. K. Y. Lam, "The survival of a biological system to mixed radiations." Radiat. Res., vol. 110, pp. 232-243, 1987.

[9] D. E. Lea, Actions of radiation on living cells. 2nd edition, Cambridge Univ. Press, New York 1955.

[10] K. H. Chadwick and H. P. Leenhouts, "A molecular theory of cell survival," Phys. Med. Biol. vol. 18, pp. 78-87,1973.

[11] C. A. Tobias, "The repair-misrepair model in radiobiology: comparison to other models," Radiat. Res., vol. 104, pp S77-95, 1985.

[12] D. T. Goodhead, "Saturable repair models of radiation action in mammalian cells," Radiat. Res. vol. 104, pp. S58-67, 1985.

[13] S. B. Curtis, "Lethal and potentially lethal lesions induced by radiation – a unified repair model." Radiat. Res. vol. 106, pp 252-271, 1986.

[14] N.tilly, A.Brahme, J. Carlsson and B. Glimelius., " Comparison of cell survival models for mixed LET radiation," Int. J. Radiat. Biol., vol. 75(2), pp 233-243, 1999.

[15] K. M. Prise, M. Pinto, H. C. Newman and B. D. Michael, "A review of studies of ionizing radiation-induced double-strand break clustering," Radiat. Res. vol. 156, pp. 572-576, 2001.

[16] F.A. Cucinotta, H.Nikjoo, D.T. Goodhead., " The effect of delta rays on the number of particle-track traversals per cell in laboratory and space exposures." Radiat. Res., vol. 150, pp115-119, 1998.

[17] E. Hoglund and B.Stenerlow, " induction and rejoining of DNA double-strand breaks in normal human skin fibroblasts after exposure to radiation of different linear energy transfer: possible roles of track structure and chromatin organization," Radiat. Res., vol. 155, pp 818-825, 2001.

[18] H. Nikjoo, P. O'Neill, W. E. Wilson and D. T. Goodhead, "Computational approach for determining the spectrum of DNA damage induced by ionizing radiation," Radiat. Res. vol. 156, pp. 577-583, 2001.

[19] E. Pastwa, R. D. Neumann, K. Mezhevaya and T. A. Winters, "Repair of radiation-induced DNA double-strand breaks is dependent upon radiation quality

and the structural complexity of double-strand breaks," Radiat. Res. vol. 159, pp. 251-261, 2003.

[20] W. R. Holley and A. Chatterjee, "Clusters of DNA damage induced by ionizing radiation: formation of short DNA fragments. I. theoretical modeling," Radiat. Res. vol. 145, pp. 188-199, 1996.

[21] B. Rydberg, "Clusters of DNA damage induced by ionizing radiation: formation of short DNA fragments. II. experimental detection," Radiat. Res. vol. 145, pp. 200-209, 1996.

[22] W. Friedland, P. Jacob, P. Bernhardt, H. G. Paretzke and M. Dingfelder, "Simulation of DNA damage after proton irradiation," Radiat. Res. vol. 159, pp. 401-410, 2003.

[23] K.G. Hofer, N.V. Loon, M. H. Schneiderman and D.E.Charlton. "The Paradoxical nature of DNA damage and cell death induced by ^{125}I Decay," Radiat. Res. vol. 130, pp. 121-124, 1992.

[24] K.G. Hofer and Shi-Ping Bao. "Low-LET and High_LET radiation action of ^{125}I decays in DNA: effect of cysteamine on micronucleus formation and cell killing," Radiat. Res. vol. 141, pp. 183-192, 1995.

[25] K. G. Hofer, X. Lin and M. H. Schneiderman, "Paradoxical effects of iodine-125 decays in parent and daughter DNA: A new target model for radiation damage," Radiat. Res. vol. 153, pp. 428-435, 2000.

[26] M. H. Schneiderman, K. G. Hofer and G. S. Schneiderman, "Targets for radiation induced cell death: When DNA damage doesn't kill." Radiat. Res. vol. 155, pp. 529-535, 2001.

[27] D. Frankenberg, M. Frankenberg-Schwager, M. Bloecher and R. Harbich. "Evidence for DNA double strand breaks as the critical lesion in yeast cells irradiated with sparsely or densely ionizing radiation under oxic or anoxic conditions," Radiat. Res., vol. 88, pp. 524-532, 1981.

[28] D.T. Goodhead. “Initial events in the cellular effects of ionizing radiations: clustered damage in DNA,” Int. J. Radiat. Biol., vol. 65(1), pp. 7-17, 1994.

[29] H. Nikjoo, P.O’Neill, D.T. Goodhead and M. Terrissol. “Computational modeling of low-energy electron-induced DNA damage by early physical and chemical events,” Int. J. Radiat. Biol, vol. 71(5), pp. 467-483, 1997.

[30] V. Michalik and D. Frankenberg. “Two types of double-strand breaks in electron and photon tracks and their relation to exchange-type chromosome aberrations,” Radiat. Environ Biophys, vol. 35, pp. 163-169, 1996.

[31] D.T. Goodhead, D.J. Brenner. “Estimation of a single property of low LET radiations which correlates with biological effectiveness,” Phys. Med. Biol., vol. 28, pp 485-492, 1983.

[32] W. Friedland, P.Jacob, H.G. Paretzke, M.Merzagora and A. Ottolenghi. “Simulation of DNA fragment distributions after irradiation with photons,” Radiat. Environ. Biophys. vol. 38, pp 39-47, 1999.

[33] P.E. Bryant, C.Jones, G. Armstrong, M.Frankenberg-Schwager and D. Frankenberg. “Induction of chromatid breaks by carbon K-shell Ultrasoft X-rays,” Radiat. Res. vol. 159, pp 247-250, 2003.

[34] B. Fayard, A. Touati, F. Abel, M.A. Herve du Penhoat, et al. “Cell inactivation and double-strand breaks: the role of core ionizations, as probed by ultrasoft X rays.” Radiat. Res. vol. 157, pp128-140, 2002.

[35] G. Taucher-Scholz, J. Heilmann and G. Draft. “Induction of DNA strand breaks by heavy ions,” Nucl. Instr. Meth. Phys. Res. vol. B107, pp 318-322, 1996.

[36] H. Nikjoo, P.O’Neill, M. Terrissol and D.T. Goodhead. “Quantitative modeling of DNA damage using Monte Carlo track structure method,” Radiat. Environ. Biophys. vol. 38, pp31-38, 1999.

[37] D.T. Goodhead, H. Nikjoo. “Track structure analysis of ultrasoft X-rays compared to high- and low-LET radiations,” Int. J. Radiat. Biol., vol. 55, pp. 513-529, 1989.

[38] E. Hoglund, E. Blomquist, J. Carlsson and B. Stenerlow. “DNA damage induced by radiation of different linear energy transfer: initial fragmentation,” Int. J. Radiat. Biol., vol. 76(4), pp 539-547, 2000.

[39] H.C. Newman, K.M. Prise, M.Folkare and B.D. Michael. “DNA double-strand break distributions in X-ray and alpha-particle irradiated V79 cells: evidence for non-random breakage,” Int. J. Radiat. Biol., vol.71, pp 347-363,1997.

[40] M. Lobrich, P.K.Cooper and B. Rydberg. “Non-random distribution of DNA double-strand breaks induced by particle irradiation,” Int. J. Radiat. Biol., vol. 70, pp. 493-503, 1996.

[41] B. Rydberg, L. Heibronn, W.R. Holley, M.Lobrich, C. Zeitlin, A.Chatterjee and P.D. Cooper. “Spatial distribution and yield of DNA double-strand breaks induced by 3-7 MeV helium ions in human fibroblasts,” Radiat. Res., vol. 158, pp. 32-42, 2002.

[42] J. S. Bedford and W.C. Dewey. “Radiation research society 1952-2002: Historical and current highlights in radiation biology: has anything important been learned by irradating cells?, ” Radiat. Res., vol. 158, pp 251-291, 2002.

[43] M. Frankenberg-Schwager., “Induction, repair and biological evidence of radiation-induced DNA lesions in eukaryotic cells,” Radiat. Environ. Biophys. vol. 29, pp 272-291,1990.

[44] M. Frankenberg-Schwager, D. Frakenberg, R. Harbich and C. Adamczyk. “A comparative study of rejoining of DNA double-strand breaks in yeast irradiated with 3.5 MeV α-particles or with 30 MeV electrons,” Int. J. Radiat. Biol. vol. 57, pp 1151-1168, 1990.

[45] B.Stenerlow, E. Hoglund, J.Carlsson and E. Blomquist. “Rejoining of DNA fragments produced by radiation of different linear energy transfer,” Int. J. Radiat. Biol. vol.76(4), pp 549-557, 2000.

[46] M. Lobrich, B. Rydberg and P.K. Cooper. "DNA double-strand breaks induced by high-energy neon and iron ions in human fibroblasts.II. Probing individual Notl Fragments by hybridization," Radiat. Res. vol. 139, pp 142-151, 1994.

[47] M. Lobrich, P.K.Cooper and B.Ryderg. "Joining of correct and incorrect DNA ends at double-strand breaks produced by high-linear energy transfer radiation in human fibroblasts," Radiat. Res. vol.150, pp 619-626, 1998.

[48] B. Fouladi, C.A. Waldren. B.Rydberg and P.K. Cooper. "Comparison of repair of DNA double-strand breaks in identical sequences in primary human fibroblast and immortal hamster-human hybrid cells harboring a single copy of human chromosome11," Radiat. Res., vol. 153, pp 795-804, 2000.

[49] E. Pastwa, R. D. Neumann, K. Mezhevaya and T. A. Winters, "Repair of radiation-induced DNA double-strand breaks is dependent upon radiation quality and the structural complexity of double-strand breaks," Radiat. Res. vol. 159, pp. 251-261, 2003.

[50] W.C. Dewey, C.C. Ling. and R.E. Meyn. "Radiation-induced apoptosis: relevance to radiotherapy," Int. J. Radiat. Oncol. Biol. Phys. vol. 33(4), pp 781-796, 1995.

[51] K.J. Weber. "Models of cellular radiation action-an overview.", Quantitative mathematical models in radiation biology. Springer-Verlang Berlin Heidelberg, 1988.

[52] G. J. Neary, R. J. Preston, and J. R. K. Savage. "Chromosome aberrations and the theory of RBE. III. Evidence from experiments with soft x-rays, and a consideration of the effects of hard x-rays," Int. J. Radiat. Biol., vol.12, pp. 317-345, 1967.

[53] R.K. Sachs, P.Hahnfeld and D.J. Brenner. "The link between low-LET dose-response relations and the underlying kinetics of damage production/ repair/ misrepair," Int. J. Radiat. Biol., vol. 72(4), pp. 351-374, 1997.

[54] G.J. Neary. “Chromosome aberrations and the theory of RBE. I. General consideration,” Int.J. Radiat. Biol., vol. 9, pp 477 , 1965.

[55] A. M. Kellerer and H.H. Rossi. “ The theory of dual radiation action,” Curr. Top. Radiat. Res. Vol. 8, pp 85, 1972.

[56] A. M. Kellerer and H. H. Rossi, “A generalized formulation of dual radiation action,” Radiat. Res. vol. 75, pp 471-488, 1978.

[57] C.A. Tobias, E.A. Blakely, F.Q. H. Ngo and T.C.H.Yang. “The repair-misrepair model of cell survival,” Radiation Biology in Cancer Research, Edited by R.E. Meyn and H.R. Withers; pp.195-230. Raven Press, New York.

[58] S.B. Curtis. “The lethal and potentially lethal Model- A review and recent development,” Quantitative Mathematical Models in Radiation Biology. J.Kiefer(Ed.), Springer-Verlag Berlin Heidelberg, 1988.

[59] H. H. Rossi and M. Zaider, “Compound dual radiation action, I. General Aspects,” Radiat. Res. vol. 132, pp. 178-183, 1992.

[60] H.H.Rossi. “Geometric domains in cellular radiobiology,” Radiat. Protect. Dos, vol. 52(1-4), pp 9-12, 1994.

[61] D. G. Goodhead, “An assessment of the role of microdosimetry in radiobiology,” Radiat. Res. vol. 91, pp 45-76, 1982.

[62] M.C. Joiner. “Models of radiation cell killing”. pp. 52-57 in Basic Clinical Radiobiology, Edited by G. Gordon Steel, Oxford University Press Inc.

[63] K.M. Rrise, G. Ahnstrom, M.Belli, J. Carlsson and D. Frankenberg et al. “A review of dsb induction data for varying quality radiation. Int. J. Radiat. Boil., vol. 74, pp 173-184, 1998.

[64] H. Nikjoo et al. “Track structure in radiation biology: theory and applications,” Int J. Radiat. Biol., vol. 73(4), pp 355-366, 1998.

[65] D.T. Goodhead, J. Thacker and R.Cox. "Effects of radiations of different qualities on cells: molecular mechanisms of damage and repair," Int. J. Radiat. Biol., vol. 63(5), pp 543-556, 1993.

[66] R.D. Stewart. "Two-lesion kinetic model of double-strand break rejoining and cell killing," Radiat. Res., vol.156, pp 365-378, 2001.

[67] M. Guerrero, R.D. Stewart, J.Z. Wang and X.A. Li., "Equivalence of the linear-quadratic and two-lesion kinetic models," Phys. Med. Biol., vol.47, pp 3197-3209, 2002.

[68] C. K. Wang and X. Zhang, "Compound dual radiation action theory for ^{252}Cf brachytherapy," Radia. Prot. Dos., vol. 110(1-4), pp 801-806, 2004.

[69] R.B. Hawkins., " A microdosimetric-kinetic model for the effect of non-poisson distribution of lethal lesions on the variation of RBE with LET," Radiat. Res., vol. 160, pp 61-69, 2003.

[70] R.B. Hawkins., " A microdosimetric-kinetic theory of the dependence of the RBE for cell death on LET," Med. Phys., vol. 25(7), pp 1157-1170, 1998.

[71] J.T. Lett, "Damage to DNA and chromatin structure from ionizing radiations, and the radiation sensitivities of mammalian cells." Progress in Nucleic Acid Research and Molecular Biology, vol.39, pp 305-352,1990.

[72] C.M. de Lara, M.A. Hill, T.J. Jenner, D. Papworth and P.O'Neill., "Dependence of the yield of DNA double-strand breaks in Chinese Hamster V79-4 Cells on the photon energy of Ultrasoft X-rays," Radiat. Res., vol. 155. pp 440-448, 2001.

[73] B. Stenerlow, E. Hoglund and J. Carlsson. "DNA fragmentation by charged particle tracks," Adv. Space Res., vol. 30(4), pp 859-863, 2002.

[74] D. T. Goodhead, J. Thacker and R. Cox, " Effectiveness of 0.3 keV carbon ultrasoft X-rays for the inactivation and mutation of cultured mammalian cells," Int. J. Radiat. Biol. vol. 36, pp 101-116, 1979.

[75] M. R. Raju, S. G. Carpenter, J. J. Chemielewski, M. E. Schillaci, M. E. Wilder, J. P. Freyer, N. F. Johnson, P. L. Schor, R. J. Sebring and D. T. Goodhead, "Radiobiology of ultrasoft X rays. I. Cultured hamster cells (V79)," Radiat. Res. vol. 110, pp 396-412, 1987.

[76] L. Hlatky, R. K. Sachs, M. Vazquez, and M. N. Cornforth, "Radiation-induced chromosome aberrations: insights gained from biophysical modeling," BioEssays vol. 24, pp 714-723, 2002.

[77] D. E. Watt, Quantities for dosimetry of ionizing radiations in liquid water, Taylor & Francis, 1996.

[78] D. T. Goodhead, "The initial physical damage produced by ionization radiations," Int. J. Radiat. Biol., vol. 56(5), pp 623-634, 1989.

[79] N. J. McNally, J. De Ronde and M. Folkard, "Interaction between X-ray and α-particle damage in V79 cells," Int. J. Radiat. Biol., vol. 53(6), pp 917-920, 1988.

[80] S. Suzuki, "Survival of Chinese hamster V79 cells after irradiation with a mixture of neutrons and ^{60}Co γ rays: experimental and theoretical analysis of mixed irradiation," Radiat. Res., vol 133, pp 327-333, 1993.

[81] M. Belli, A. Campa and I. Ermolli, "A semi-empirical approach to the evaluation of the relative biological effectiveness of therapeutic proton beams: the methodological framework," Radiat. Res., vol. 148, pp 592-598, 1997.

[82] M. Folkard, K. M. Prise, B. Davies, M. J. Roper and B. D. Michael, "The irradiation of V79 mammalian cells by protons with energies below 2 MeV, Part I: Experimental arrangement and measurement of cell survival," Int J. Radiat. Biol., vol. 56 (3), pp 221-237, 1989.

[83] D. E. Charlton, D. T. Goodhead, W. E. Wilson, and H. G. Paretzke, Energy deposition in cylindrical volumes: (a) protons energy 0.3 MeV to 4.0 MeV, (b) alpha particles energy 1.2 MeV to 20.0 MeV. M.R.C. Radiobiology Unit Monograph, Chilton, U.K., July 1985.

[84] H. Nikjoo, D. T. Goodhead, D. E. Charlton, and H. G. Paretzke, Energy deposition by monoenergetic electrons in cylindrical volumes., M.R.C. Radiobiology Unit Monograph, Chilton, U.K., March 1994.

[85] H. Nikjoo, D. T. Goodhead, D. E. Charlton, and H. G. Paretzke, "Energy deposition in small cylindrical targets by ultrasoft x-rays," Phys. Med. Biol., vol. 34(6), pp 691-705, 1989.

[86] F. H. Attix., Introduction to radiological physics and radiation dosimetry, pp 475-480, John Wiley & Sons, Inc., 1986.

[87] F. T. Kuchnir, C. J. Vyborny and L. S. Skaggs., " A new method for determining the neutron response function of 'neutron insensitive' dosimeters. Method and preliminary determinations," Radiology, vol. 116, pp 217-219. 1975.

[88] MCNP-A general Monte Carlo N-particle transport code, version 5, " volume II: users guide", Los Alamos, 2003.

[89] Herman Cember., Introduction to health physics, third edition., pp 518-520, The McGraw-Hill companies, Inc. 1996.

[90] R.C. Martin, R.R. Laxson, J.H. Miller, J.G. Wierzbick, M.J. Rivard, and D.L. Marsh. "Development of high-activity ^{252}Cf sources for neutron brachytherapy," Applied Radiation and Isotopes," vol. 48 (10-12), pp 1567-1570, 1997.

[91] Y. Maruyama, J.R. van Nagell, J. Yoneda, E.S. Donaldson, H. H. Gallion, D. Powell and R. J. Kryscio. "A review of californium-252 neutron brachytherapy for cervical cancer. Cancer," vol. 68 (6), pp. 1189-1197, 1991.

[92] H. B. Kal. "Review of RBE and OER values for Cf-neutrons," Nucl. Sci. Appli., vol. 2, pp 303-316, 1986.

[93] H.Yamashita, T. Wada, T. Dokiya and S. Hashimoto., "Physical and biological dosimetries of Cf-252 radiation," Nucl. Sci. Appli., vol. 2, pp 345-367, 1986.

[94] N. J. McNally, J. De Ronde, M. Hinchliffe., "Survival of V79 cells following simultaneous irradiation with X-rays and neutrons in air or hypoxia," Int. J. Radiat. Biol., vol. 48 (5), pp 847-855, 1985.

[95] N.J. McNally, J. De Ronde, M. Folkard., "Interaction between X-ray and α-particle damage in V79 cells," Int. J. Radiat. Biol., vol. 53 (6), pp 917-920 ,1988.

[96] H.E. Jonhs and J.R. Cunningham, The physics of radiology, pp 686-187, Fourth Edition. Charles C Thomas, Publisher, 1983.